National Geohazards Mapping in Europe: Interferometric Analysis of the Netherlands

David Gee [a, b*], Andrew Sowter [b], Stephen Grebby [a], Ger de Lange [c], Ahmed Athab [b], Stuart Marsh [a]

[a] Nottingham Geospatial Institute, University of Nottingham, Nottingham, NG7 2TU

[b] Geomatic Ventures Limited, Nottingham Geospatial Building, Nottingham, NG7 2TU

[c] Deltares, Post box 85467, 3508 AL Utrecht, The Netherlands

* Corresponding author: david.gee@nottingham.ac.uk

Abstract

The launch of Copernicus, the largest Earth Observation program to date, is significant due to the regular, reliable and freely accessible data to support space-based geodetic monitoring of physical phenomena that can result in natural hazards. In this study, wide area interferometric synthetic aperture radar (InSAR) capability is demonstrated by processing 435 Copernicus Sentinel-1 C-Band SAR images (May 2015 – May 2017) using the Intermittent Small Baseline

Subset (ISBAS) method to produce a wide-area-map (WAM) covering 53,000 km^2 of the Netherlands, Belgium and Germany. The ISBAS-WAM contains over 19 million measurements, achieving a ground coverage of 94%. The retrieval of measurements over soft surfaces (i.e. agricultural fields, forests and wetlands) was crucial due the dominance of non-urban land cover. A statistical analysis of the velocities reveals that intermittently coherent measurements in rural areas can provide reliable, additional deformation information with a very high degree of confidence (5σ), which spatially correlates to known deformation features associated with compressible soils, infrastructure settlement, peat oxidation, gas production, salt mining and underground and opencast mining. The spatial distribution of deformations concurs with independent data sources, such as previous persistent scatterer interferometry (PSI) deformation maps, models of subsidence and settlement susceptibility, and quantitatively with GPS measurements over the Groningen gas field.

Remotely derived deformation products, with near complete spatial coverage, provide a powerful screening tool for mitigation and remediation of geological and geotechnical issues to help in the protection of assets, property and life. The ISBAS-WAM demonstrates that routine generation of such products on a continental scale is now theoretically achievable, given the establishment of the Copernicus programme and the development of state-of-the-art InSAR methods, such as ISBAS.

Keywords

National Geohazard Mapping; Surface Deformation; Interferometric SAR; Intermittent SBAS; Sentinel-1; Copernicus Programme

Research Highlights

- ISBAS InSAR was used to produce a national deformation map with 94% coverage.
- Pixels in rural areas provided reliable measurements at the 5σ level.
- Motions were attributed to six main phenomena.
- National deformation maps can provide critical information on potential geohazards.

1. Introduction

In Europe, the European Space Agency (ESA) and the European Union (EU) have supported a large range of projects that have demonstrated the feasibility of space technologies to monitor geohazards across the continent, although primarily those affecting cities. Examples of such projects include ESA-Terrafirma (2003 – 2012) (Adam *et al.*, 2009), EU-FP7-Subcoast (2010 – 2013) (Gruijters & van der Krogt, 2013), EU-FP7-PanGeo (2011 – 2014) (Capes, 2012) and EU-FP7-PROTHEGO (2015 – 2018) (Themistocleous *et al.*, 2016). Satellite-based interferometric synthetic aperture radar (InSAR) has played a central role in all of these projects as it is capable of measuring and monitoring a wide range of geohazards including landslides (Bayer *et al.*, 2017), tectonics (Colesanti *et al.*, 2003) and volcanology (Hooper *et al.*, 2004), in addition to ground motion associated with anthropogenic activity such as oil and gas operations (Castelletto *et al.*, 2013), carbon capture and storage (Rohmer *et al.*, 2015), mining (Gee *et al.*, 2017), civil engineering works (Marshall *et al.*, 2018) and groundwater abstraction (Boni *et al.*, 2015).

The success of the value-added products derived from the aforementioned ESA and EU projects demonstrate that InSAR has reached a level of maturity where national-scale land motion maps are now feasible. There have been a number of demonstrations of wide-area mapping capability (e.g. Adam *et al.*, 2011; Chaussard *et al.*, 2013; Chaussard *et al.*, 2014), and full maps of the Netherlands (Cuenca *et al.*, 2011; Hanssen & Cuenca, 2012) and Italy (Costantini *et al.*, 2017) have been generated using persistent scatterer interferometry (PSI) techniques. However, PSI solutions are primarily limited to mapping surface deformation in urbanised areas, which comprise only 12% and 5% of the surface area of the Netherlands and Italy, respectively (European Environment Agency, 2012). Furthermore, at the time of these earlier studies, ample SAR data was generally not available and, in some cases, marginal for reliable InSAR analysis. Consequently, the PSI results required interpolation and/or assimilation with ancillary data to achieve nationwide coverage. For example, Cuenca *et al.* (2011) utilized ERS 1/2 and ENVISAT SAR data alongside supplementary geodetic measurements from levelling and GPS for the period 1992–2011. Since then, advances have been made in state-of-the-art InSAR processing techniques, such as the Intermittent Small Baseline Subset (ISBAS) method (Sowter *et al.*, 2013; Sowter *et al.*, 2016), which can derive ground motion measurements over urban and rural environments alike. Moreover, the availability and accessibility of SAR data has also vastly improved with the launch of the Copernicus programme.

Copernicus is an EU programme, managed and coordinated by the European Commission, which was founded to develop European information services based on *in situ* and satellite Earth Observation (EO) data. Copernicus is served via a group of satellite missions (Sentinels) which deliver regular, reliable, near real–time data that are provided freely to all end users (i.e. commercial and institutional). It will eventually be served by twenty satellites as part of 6 missions, the first of which, Sentinel-1a, was launched in April 2014. Sentinel-1 is an imaging radar mission carrying a C-Band (5.405 GHz) SAR instrument at an altitude of 693 km in a near-polar sun-synchronous orbit. The two-satellite constellation currently maintains a conflict-free repeat pass of 6 days over Europe, representing a significant improvement in reliability and revisit time over legacy SAR missions (Torres *et al.*, 2012). The technical and operational capabilities of the mission fully support interferometric processing and it therefore has potential to underpin cost-effective, wide area geohazard mapping across Europe and, indeed, anywhere in the world, for the foreseeable future.

Sentinel-1 is already showing significant promise in supporting national geohazard programmes, which require products like maps of surface deformation to be generated in a systematic semi-automated process and methodically kept up to date with new data (van der Meulen *et al.,* 2013). This necessitates the operational processing of large volumes of EO data on a regular basis. Currently, over 8 Petabytes per year are acquired, processed and disseminated by the Copernicus Programme which presents new challenges in the era of big EO data. The volume, frequency, variety and complexity of data outstrips conventional computing and storage capabilities and therefore new solutions are required to support EO applications.

Given this abundance of new EO data and the need for a semi-automated operational approach to generating national-scale surface displacement information, this study aims to demonstrate the potential of Copernicus Sentinel-1 SAR data for geohazard mapping and monitoring in Europe. This is achieved through the generation of an Intermittent Small Baseline Subset Wide-Area-Map (ISBAS-WAM) covering the Netherlands and extending into neighbouring areas of Belgium and Germany (totalling 53,000 km^2), without the need for interpolation or integration with ancillary data. The ISBAS-WAM highlights ground deformation associated with a range of potential geohazards capable of posing a risk to both infrastructure and society, which are subsequently discussed in detail. Finally, the processing requirements for a full Europe-wide deformation map are calculated to determine the opportunity and challenges Copernicus presents for future operational monitoring services.

2. The Netherlands

2.1 Land Cover

The Netherlands has a total land mass of ~33,500 km^2 and is dominated by rural areas which comprise 86% of the total surface area (Figure 1). Agriculture (73%) dominates land use in the rural landscape, with the remainder comprising various forested and semi-natural areas (12%) and wetlands (1%). Artificial surfaces in the form of housing, built structures and transport infrastructure make up 14% of the total land cover, evident in pockets of distinct urban clusters. Urban developments are most prominent between Amsterdam and Rotterdam in the Randstad megalopolis in the west, with notably less development in the eastern and northern provinces.

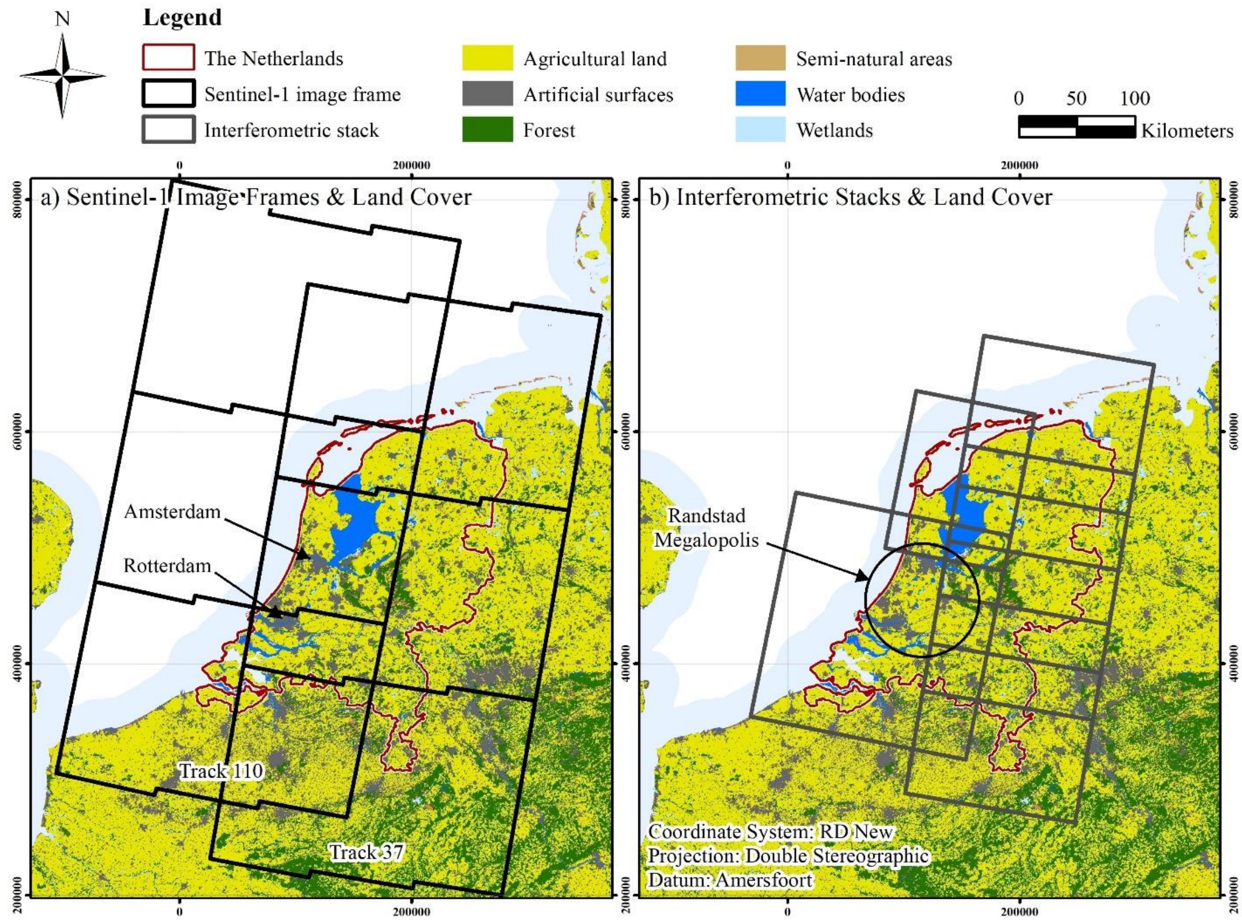

Figure 1. CORINE Land Cover inventory (European Environment Agency, 2012): (a) Sentinel-1 image frames (b) Interferometric stacks. European Environment Agency © 2012.

2.2. Geology

The Netherlands is located on the south-eastern edge of the Cenozoic North Sea basin and consists of three distinct domains: a Holocene coastal barrier formed of sand dunes in the west, a lowland coastal and fluvial plain, and a relatively higher inland area of Pleistocene deposits that extends to the east (De Mulder, 1994; Figure 2). Covering about half of the country, the coastal and fluvial plain lies approximately at and below sea level and consists mainly of sand, clay and peat. Peat beds, which can be up to 8 m thick, are geotechnically the weakest part of the Holocene succession. Such deposits, along with younger soft Holocene clays, are particularly predisposed to settlement and compaction. Holocene sands deposited in tidal channels are very loosely packed and often exhibit porosities greater than 40%, consequently, such sands can be instable and prone to liquefaction (De Mulder, 1994). The Pleistocene deposits in the east are predominantly sandy soils that are glacial, fluvial and aeolian in origin. While generally flat, these deposits gently slope upwards to an elevation of 20 m above mean sea level in the east and south, although ice-pushed ridges can locally reach heights of 100 m (De Mulder, 1994; van der Meulen *et al.*, 2013).

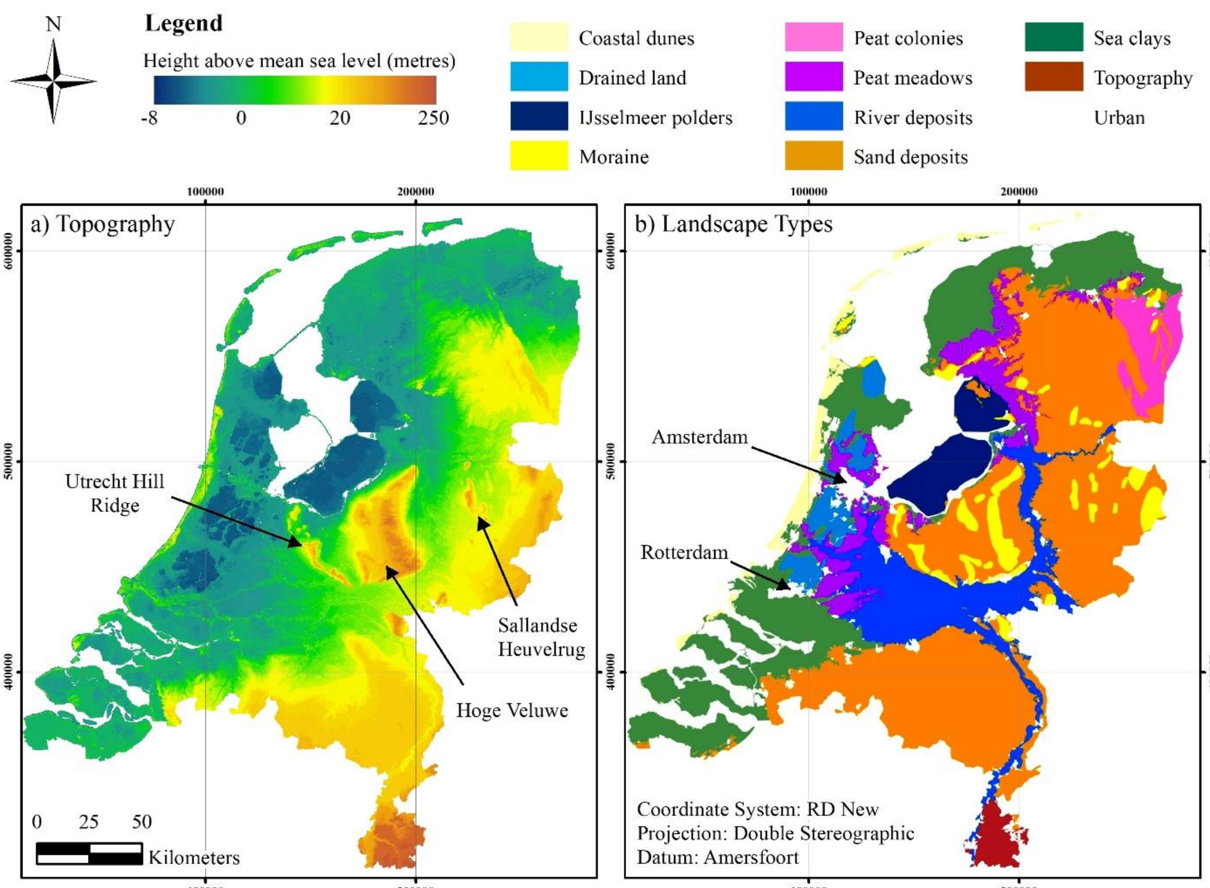

Figure 2. (a) Topography and (b) Landscape types of the Netherlands.

2.3. Geohazards in the Netherlands

Due to its low-lying geographical setting and sedimentary composition, flooding and land subsidence are the predominant geohazards in the Netherlands. Deformations can be broadly classified into two categories: shallow Holocene motions (up to 30 metres deep) induced by peat oxidation, sediment compaction and dewatering; and deeper sources driven by gas production, mining, tectonics and underground water pumping (Hanssen & Cuenca, 2012). The combination of sea level rise and land subsidence increases the risk of flooding, salt water contamination of low-lying aquifers and surface water and the cost of maintaining drained agricultural farmland in low-lying coastal areas. If it were not for anthropogenic (e.g. dikes and water pumps) and natural defences (i.e. sand dunes), over 60% of the country would be submerged at high tide and most of the sub-datum area would inundate due to upward seepage (De Mulder, 1994). Soil compaction increases the need for pumping, which in turn increases rates of subsidence, hence, the detrimental circle the Netherlands is locked into. Differential motion of soils in the shallow subsurface are hazardous to built structures and surface and sub-surface infrastructure. Damage severity depends on the velocity of differential motions which is controlled by the spatial distribution and thickness of soft soil layers, groundwater regime and the presence or state of foundations (Peduto *et al.*, 2017). Furthermore, the peatlands that dominate the Dutch lowlands act as large carbon stores, and drainage of such environments contributes to increasing global temperatures and climate change (Erkens *et al.*, 2016).

Secondary hazards include induced seismicity from the extraction of natural gas, which has caused recent public concern following the 2012 magnitude 3.6 Huizinge earthquake in Groningen (van Thienen-Visser *et al.*, 2018). Reservoir compaction is considered to be a driving force of induced seismicity in the Groningen field (Bourne *et al.*, 2014). Accordingly, there are extensive legal, technical and organizational frameworks to ensure subsidence remains within predefined limits and is openly communicated to the public (de Waal *et al.*, 2012).

3. Processing

3.1 The ISBAS Method

A variety of PSI (e.g. Ferretti *et al.*, 2001; Hooper *et al.*, 2004) and small baseline methods (e.g. Berardino *et al.*, 2002) have been shown to produce very accurate profiles of deformation over hard targets such as rocky or urban areas. However, a principal limitation of InSAR analysis is decorrelation, whereby the scattering properties of the imaged target change over time. This is common over rural settings where, due to processes such as shrink-swell and agricultural practises, scatterers within resolution elements move relative to one another. Consequently, the integration of phase difference becomes inaccurate if the change in phase is a substantial percentage of the phase cycle (Zebker & Villasenor, 1992). Approximately 86% of the surface of the Netherlands is comprised of vegetated surfaces, which constitutes a significant hindrance to obtaining a high density of surface displacement measurements and, therefore, achieving detailed spatial characterisation of deformation processes (Crosetto *et al.*, 2010).

Since the introduction of the first multi-temporal InSAR method in the late 1990's, there have been new processing algorithms that have successfully managed to increase the number and spatial density of returned InSAR measurements (e.g. Hooper, 2008; Ferretti *et al.*, 2011). The ISBAS method (Sowter *et al.*, 2013; Sowter *et al.*, 2016) is a recent development that extends the coverage of deformation measurements into rural environments to provide near complete coverage. It is an adapted version of the low-resolution SBAS algorithm (Berardino *et al.*, 2002), which computes solutions for pixels which exhibit coherence in all stacked interferograms (coherent pixels). In contrast, ISBAS relaxes the need for coherence to be maintained across all interferograms. It computes solutions for coherent pixels and pixels which exhibit coherence for a specified subset of the total multiple master interferograms (intermittently coherent pixels). The ISBAS method was employed here due to the predominance of vegetation cover, and since it has been proven to achieve accurate validated results in parts of the Netherlands (Gee *et al.*, 2016) and to enable national deformation mapping elsewhere (Sowter *et al.* 2018). For a Sentinel-1 Interferometric Wide (IW) image with a nominal spatial resolution better than 25 m, the ISBAS solution is of approximately 90 m resolution.

3.2 Data Processing

A total of 435 Sentinel-1 Level-1 IW Single Look Complex (SLC) products (May 2015 – May 2017) from descending tracks 110 and 37 were utilized (Table 1; Figure 1a). The flow diagram in Figure 3 outlines the implemented deformation mapping approach, in accordance with that of Sowter *et al*. (2018). Readers are referred to Sowter *et al.* (2013; 2016) for further details on the

ISBAS algorithm and its application to Sentinel-1 data. Six interferometric stacks (Figure 1b) were processed separately, whereby at least 30 km overlap was maintained between both neighbouring stacks in azimuth and neighbouring tracks to aid subsequent mosaicking. Two-pass low-resolution differential interferograms were generated between image pairs with restrictions of 150 m on the perpendicular orbital baseline and 365 days on the temporal baseline (Table 1). Deformation velocities were computed for pixels for which coherence (> 0.25) was maintained in ≥ 400 and 340 interferograms for tracks 110 and 37, respectively. Phase ramps attributed to orbital errors were calculated and removed, and a 90 m SRTM DEM was used to simulate and subtract phase associated with topography. Reference points were chosen in major cities where there was an abundance of highly coherent points (Figure 4a). Using a linear model of deformation, line-of-sight velocities for the time period were computed and then projected into the vertical direction by means of dividing by the cosine of the incidence angle. Whilst feasible for regional areas (e.g. Gee *et al.*, 2017), the generation of time-series at the national scale is not currently achievable due to the computational and storage demands for such a large volume of pixels generated by the ISBAS method. Software developments are ongoing to address this matter in future mosaics. A seamless deformation map was generated by mosaicking the six subsets. Individual mosaics were first generated from the two stacks in track 110 and four stacks in track 37, followed subsequently by the mosaicking of the two tracks to generate the ISBAS-WAM.

Table 1. Sentinel-1 satellite data and processing parameters used to generate the ISBAS-WAM.

Geometry	Track	Nº Frames	Acquisitions Per Frame	Start Date	End Date	Max. Orbital Baseline (Metres)	Max. Temporal Baseline (Days)	Multilooking (Azimuth: Range)	Coherence Threshold	Nº of Interferograms	Interferogram Threshold
Descending	110	3	77	5th May 2015	12th May 2017	150	365	5 : 22	0.25	1984	400
	37	3	68	12th May 2015	13th May 2017					1670	340

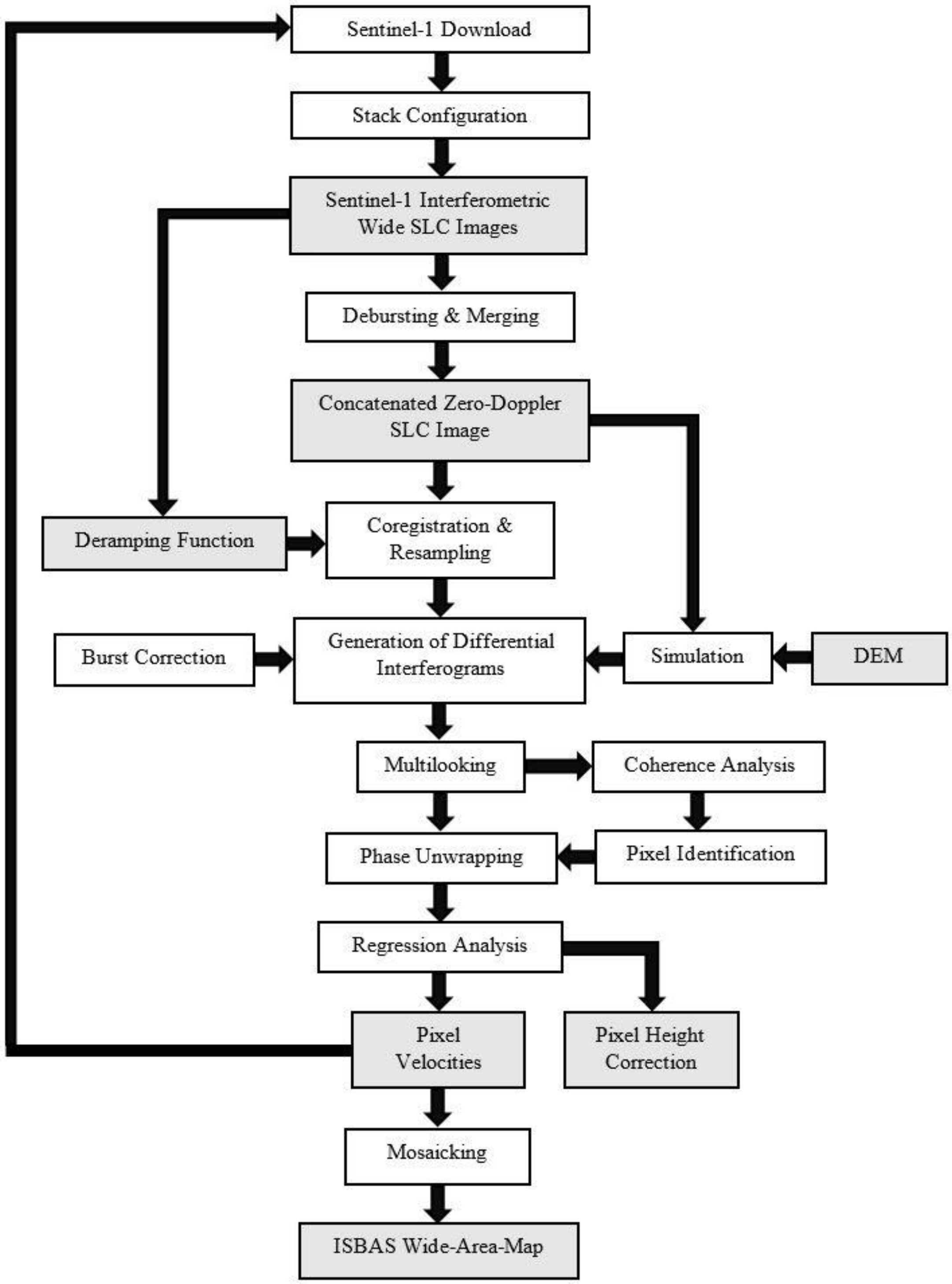

Figure 3. The deformation mapping processing chain.

4. Results

4.1 Average Velocities – National Deformation Product

The mosaicked deformation product (ISBAS-WAM) covers an area of 53,000 km^2 and reveals the average vertical ground motion for each pixel for the period May 2015 – May 2017 (Figure 4a). The pixels cover 94% of the total land surface available, with velocities computed over hard targets in towns and cities (artificial surfaces) and over soft targets in rural areas (agricultural land, forests, semi-natural areas and wetlands). It is estimated that had velocities been solely derived for coherent pixels (i.e. pixels where coherence is maintained in every differential interferogram), coverage would have only been 13% and restricted to just urban areas and transport infrastructure (Figure 4c). Figure 4d shows the velocities for the subset of intermittently coherent pixels, which evidences the crucial additional characterisation of deformation that the ISBAS method provides.

The mean density of measurements in the ISBAS-WAM is 374 solutions/km^2 (Table 2), greatest over artificial surfaces (387 solutions/ km^2) and lowest over forested areas (291 solutions/km^2). With respect to computing measurements over forested areas, although often dominated by diffuse scattering from the canopy, the ability of C-band radar to penetrate a canopy and scatter from the ground is well-known and understood to be a function of leaf area index (LAI) and incidence angle (Wang *et al.*, 1998). Indeed, InSAR has been applied successfully to monitor water level change through a moderate canopy over swamp forests (Lu & Kwoun, 2008) and the

ISBAS method has previously shown to return measurements over forested areas and map the underlying deformation (e.g. Sowter *et al.*, 2013).

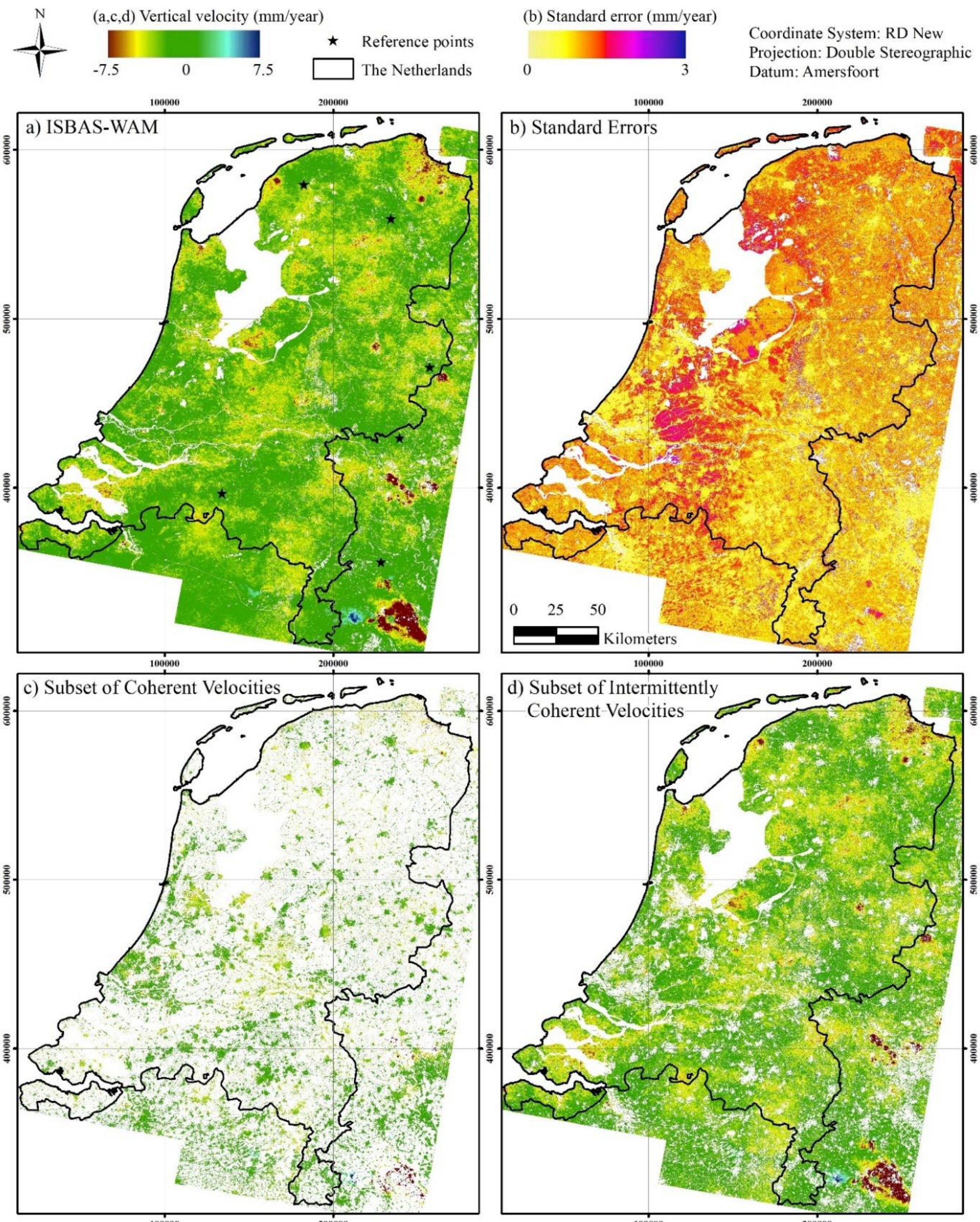

Figure 4. (a) ISBAS-WAM vertical velocities (mm/year) (b) Standard errors (mm/year) (c) Vertical velocities for the subset of coherent pixels (mm/year) (d) Vertical velocities for the subset of intermittently coherent pixels (mm/year). The complete ISBAS-WAM (a) comprises both coherent and intermittently coherent pixels.

Table 2. Ground coverage and standard errors of velocities.

Statistic	ISBAS-WAM	Coherent Pixels	Intermittently Coherent Pixels	Agricultural Land	Artificial Surfaces	Forest	Semi-natural areas	Wetlands
Ground coverage								
Nº solutions	19 775 110	3 995 561	15 779 549	13 842 700	3 642 577	1 598 758	459 437	231 638
Density (Solutions/km^2)	374	75	299	386	387	291	351	335
Standard error (millimetres / year)								
Mean	1.02	0.62	1.12	1.06	0.72	1.25	1.05	1.30
Standard deviation	0.31	0.13	0.25	0.26	0.26	0.29	0.32	0.32
Minimum	0.38	0.38	0.40	0.39	0.38	0.39	0.42	0.44
Maximum	4.60	3.50	4.60	4.30	3.51	3.77	4.60	3.78

4.2 Standard Errors

The standard error for each measurement expresses the goodness-of-fit between interferogram values and the computed linear velocity and is derived via a least-squares covariance analysis. No outlier rejection was performed in the calculation. The mean standard error was 1.02 mm/year, revealing millimetre precision across the Netherlands (Table 2; Figure 4b). Coherent pixels exhibit the lowest standard errors, on average 0.62 mm/year, while the mean standard error for intermittently coherent pixels is 1.12 mm/year. With respect to land cover types, artificial surfaces on average have the lowest standard error given the likelihood of more coherent interferograms per pixel to derive velocities; however, pixels located in agricultural and semi-natural areas exhibit approximately millimetre precision.

4.3 Statistically Significant Velocities

Observed velocities are considered reliable (i.e. 'real' and not attributed to noise) if there is a statistically significant difference between them and the population mean for a given level of confidence. Velocities that lie outside ± 3, 4 and 5 standard errors (σ) away from the population mean were determined (Table 3; Figure 5), which identifies pixels with a 99.73% (3σ), 99.994% (4σ) and 99.99994% (5σ) confidence that the velocity does not occur by chance. This corresponds to an expected frequency outside of the range of 1 in every 370, 15,787 and 1,744,278 measurements, respectively. At the 3σ, 4σ, 5σ confidence levels 2,816,698, 1,355,775 and 699,802 velocity measurements, respectively, were deemed significant, of which 57%, 48% and 43% are pixels that are characteristically intermittently coherent. Such measurements are retrieved over agricultural land, forests, semi-natural areas and wetlands as well as over artificial surfaces, and spatially correlate to known areas of deformation, as is discussed below.

Table 3. The number of statistically significant measurements at different levels of confidence.

Confidence Level	Nº of Statistically Significant Measurements							
	ISBAS-WAM	Coherent Pixels	Intermittently Coherent Pixels	Agricultural land	Artificial surfaces	Forest	Semi-natural areas	Wetlands
3σ (99.73%)	2 816 698	1 207 956	1 608 742	1 601 233	992 646	124 972	79 314	18 533
4σ (99.994%)	1 355 775	708 343	647 432	679 471	579 406	49 248	40 082	7 568
5σ (99.99994%)	699 802	396 175	303 627	326 749	326 431	23 128	20 183	3 311

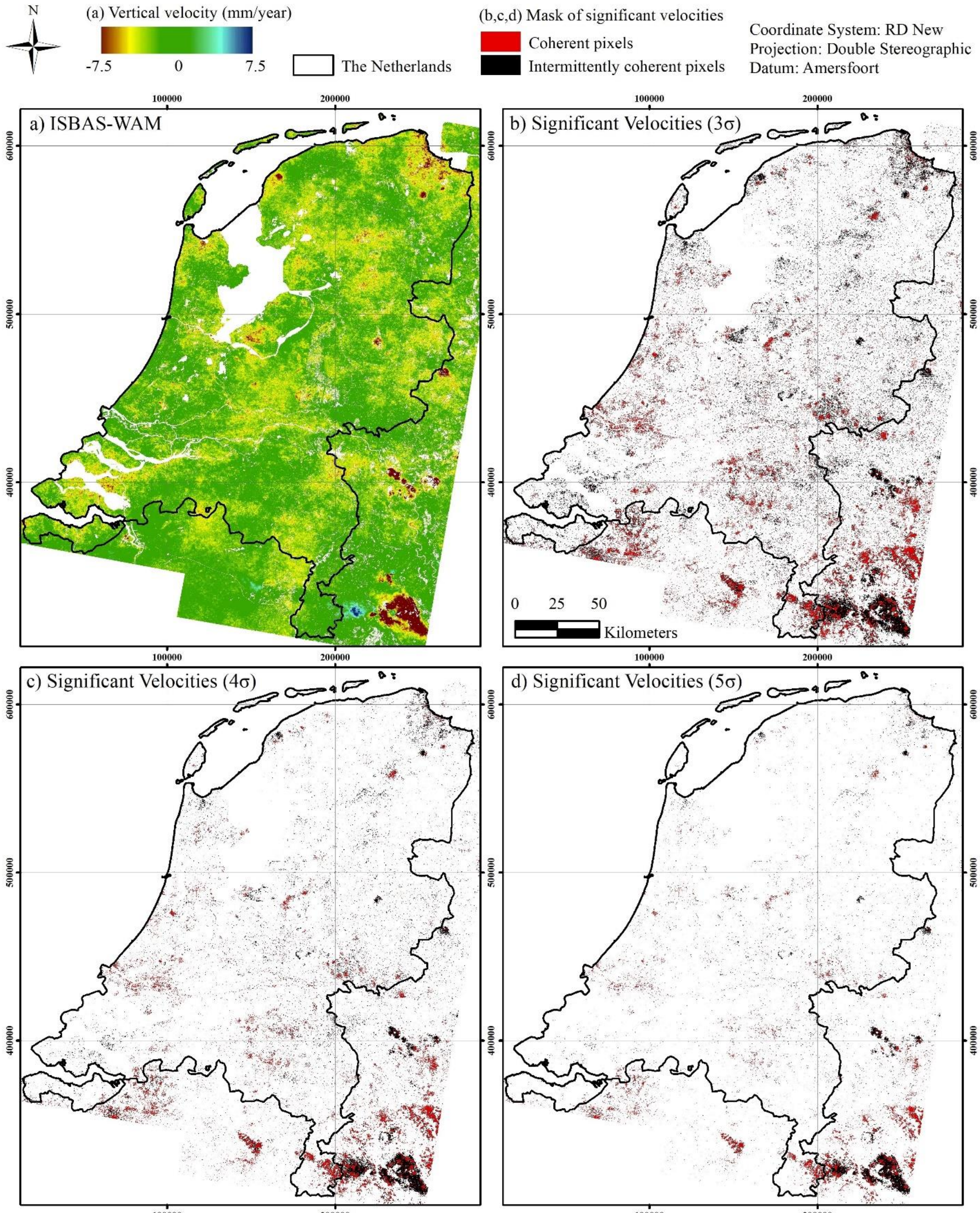

Figure 5. (a) ISBAS-WAM vertical velocities (mm/year). Mask of statistically significant velocities at: (b) 3σ (99.73%) (c) 4σ (99.994%) (d) 5σ (99.99994%) confidence levels.

5. Overview of Identified Hazards

5.1 Compressible Soils

The entirety of the Netherlands is known to be deforming in some way, whereby some areas heave but for the most part soil subsides, much of which occurs as a result of water management practises (Climate Impact Atlas, 2019). Motions in the ISBAS-WAM, in certain instances, show a high degree of spatial correlation to the Netherlands subsidence prognosis map (De Lange *et al.*, 2011; Climate Impact Atlas, 2019; Figure 6b). It identifies areas most susceptible to soil deformation under current environmental circumstances as calculated with empirical models based on the interpolation of measurements from levelling and benchmarks located in the Holocene layer. The models predict the effects of dewatering on the assumption that, despite subsidence, level indexation is followed (i.e. water levels in drainage ditches remain at a consistent level with respect to ground level) for the period 2000 – 2050, although higher rates of peat oxidation and subsidence are predicted to occur under warming climate conditions. As the predictive map covers a significantly longer time period than the ISBAS-WAM, a direct quantitative comparison requires some caution as susceptibility is an indication of potential subsidence rather than observed subsidence – which may be controlled or prevented by effective management.

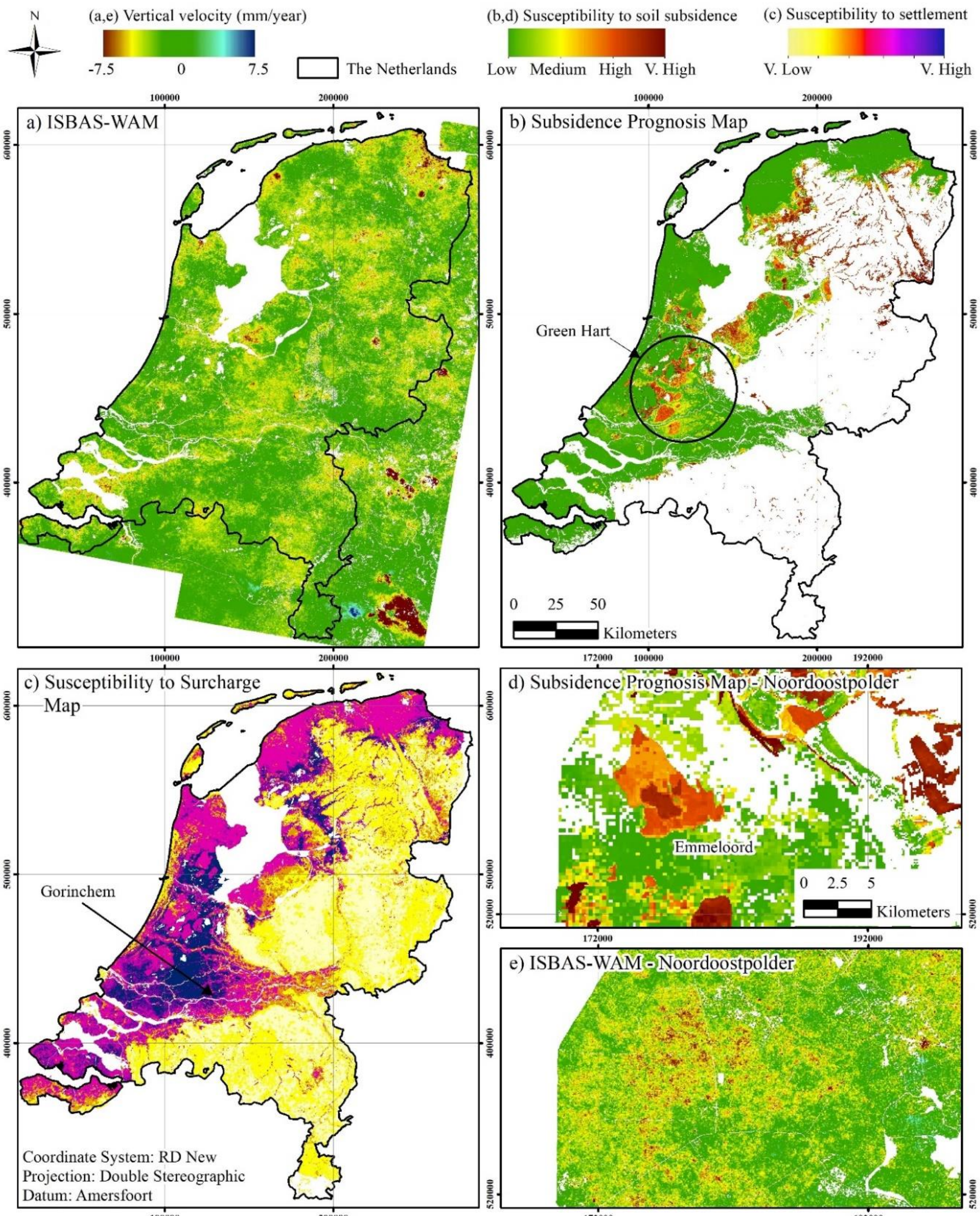

Figure 6. (a) ISBAS-WAM vertical velocities (mm/year), (b) subsidence prognosis map (De Lange *et al.*, 2011; Climate Impact Atlas, 2019) and (c) susceptibility to surcharge map of the Netherlands (De Lange *et al.*, 2012; Climate Impact Atlas, 2019). (d) Subsidence prognosis map (De Lange *et al.*, 2011; Climate Impact Atlas, 2019) and (e) ISBAS-WAM vertical velocities (mm/year) of the Noordoostpolder, Flevoland. Climate Impact Atlas © 2019.

Nonetheless, a close agreement is observed in the Flevoland polders, in the northern Noordoostpolder north-west of Emmeloord (Figure 6d,e), north-east of Dronten in the Eastern Flevoland polder and most notably in the Southern Flevoland polder near Almere (Figure 7). Eastern and Southern Flevoland is divided by a dike which runs across from Harderwijk perpendicular to the coastline west of Lelystad. The Southern Flevoland polder is more susceptible to subsidence due to the difference in age of the reclamation and the thickness of the compressible layer, which is reflected in the observed velocities in the ISBAS-WAM. Figure 7c,d demonstrates the importance of intermittently coherent pixels in characterising soil deformation with a high degree of certainty (4σ and 5σ confidence levels).

The ISBAS measurements in the 'Green Hart' (Groene Hart), a large rural area within the Dutch Randstad characterised by peat, clay and sandy soils, reveal relative stability and in cases uplift, which is contrary to predicted subsidence patterns (Figure 6a,b). Previous PSI studies (e.g. Cuenca & Hanssen, 2008) also found that this area was relatively stable in comparison with independent subsidence estimates. The predictive map is based upon susceptibility, and water levels in such low-lying areas are heavily controlled for agriculture and habitation by a complex system of drainage ditches, canals and pumping stations. The ISBAS-WAM suggests such water management practises have been effective for the period May 2015–May 2017, likely accounting for the discrepancy with the predicted subsidence.

The identification of ground motion in wetlands using traditional geodetic techniques is challenging. In the Netherlands, there is a lack of shallow benchmarks in the vicinity of benchmarks founded in the Pleistocene base (the base for the NAP datum system) and it is notoriously difficult to find consistent levelling stations of surface deformation outside of urban areas. Furthermore, attempts to monitor peat compaction utilizing PSI, such as in Cuenca & Hanssen (2008), have been hindered by decorrelation effects. The low-resolution ISBAS method does not suffer the problems of traditional geodetic methods, nor does it rely on the presence of a persistent scatterer. Hence, the retrieval of measurements on soft targets illustrates the potential to monitor and quantify the effects of water management practises on such areas – which is very valuable for policy makers defining water management strategy (Vonhögen *et al.*, 2012). The Holocene areas of the Netherlands are subject to periodicity in the ground level due to seasonal variations in ground water levels. Ground water levels are lower in the summer when soil dehydration and associated shrinkage, oxidation and deeper subsidence are most likely to occur (Vonhögen *et al.*, 2012). In this respect, InSAR time-series data is central to affirming a relationship between ground water and soft soil deformation, as is being as is being demonstrated by ongoing research efforts (e.g. UKRI, 2018).

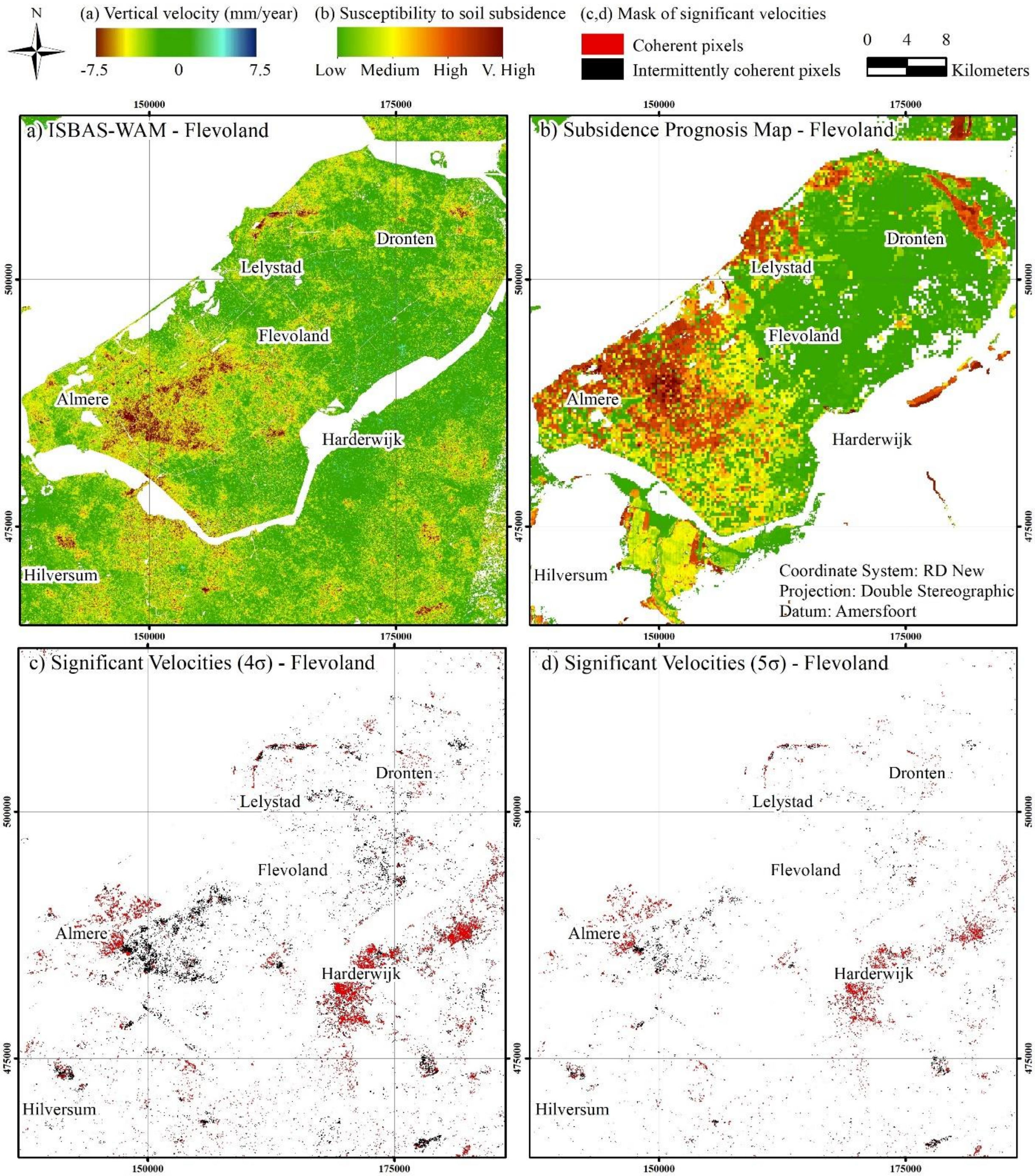

Figure 7. Flevoland: (a) ISBAS-WAM vertical velocities (mm/year) and (b) subsidence prognosis map (De Lange *et al.*, 2011; Climate Impact Atlas, 2019). Mask of statistically significant velocities at: (c) 4σ (99.994%) (d) 5σ (99.99994%) confidence levels. Climate Impact Atlas © 2019.

5.2 Infrastructure Settlement

Surface deformations in Holocene areas also relate to the compaction of sediments on which infrastructure has been built (i.e. settlement). Almost all new developments in areas of soft soils (peat, clay) are drained and raised before they are built on. Embankment is also employed to existing structures. Soil consolidates when it is raised with sand, which mainly occurs within the first months to years of placement, although residual settlement can occur decades after construction. The occurrence of soil subsidence itself is often, but not always, the reason for embankment, and such drops in elevation momentarily speed up the deformation process again due to the increased load. As a result of this self-perpetuating cycle, a layer a few metres thick has been generated in areas of weak soils in many historic city centres (Climate Impact Atlas, 2019).

Deformations in the ISBAS-WAM correlate with the susceptibility to surcharge map (De Lange *et al.*, 2012; Climate Impact Atlas, 2019; Figure 6a,c) which identifies areas susceptible to settlement after embankment. The amount of settlement after a 40-year period under a uniform load of 1 m thick sand fill is modelled; a fictitious situation which is designed to identify areas where taxing the weak subsoil has the greatest consequences, for instance to buried conduits or archaeological remains. Similarly, as with the subsidence prognosis map, a quantitative comparison is not appropriate.

There are numerous instances of deformation related to transport infrastructure, the largest areas of which occur when infrastructure crosses areas highly susceptible to settlement (Figures 8 and 9). Differential settlements often occur at the intersection of piled and embanked foundations. A 10 km stretch of deformation occurs along the railway to the north of Lelystad (Figure 8a-c). Notably, the characteristics of deformation change as the route exits north of the city and travels eastward into rural areas. Through the rural environment, the influence of the infrastructure appears to be distributed over the wider surroundings whereby deformation spreads out from the track, over 600 m in some instances. This may be attributed to the drainage system that was put in place with the embankment and the draining character of the sand embankment itself. Interestingly, this suggests that the zone of influence in a subsidence prone area extends beyond the zone of surcharge settlement. Conversely, as the track enters urban Lelystad from the north, the subsidence is confined to within a 100 m proximity of the track. This is likely due to the fact the railway embankment is surrounded by an urban area that was developed by employing a surface surcharge itself and consists of structures on piled foundations. Other notable examples occur in south Rotterdam (Figure 9c,d) and along a 10 km stretch of track between Abcoude and Breukelen (Figure 9e,f).

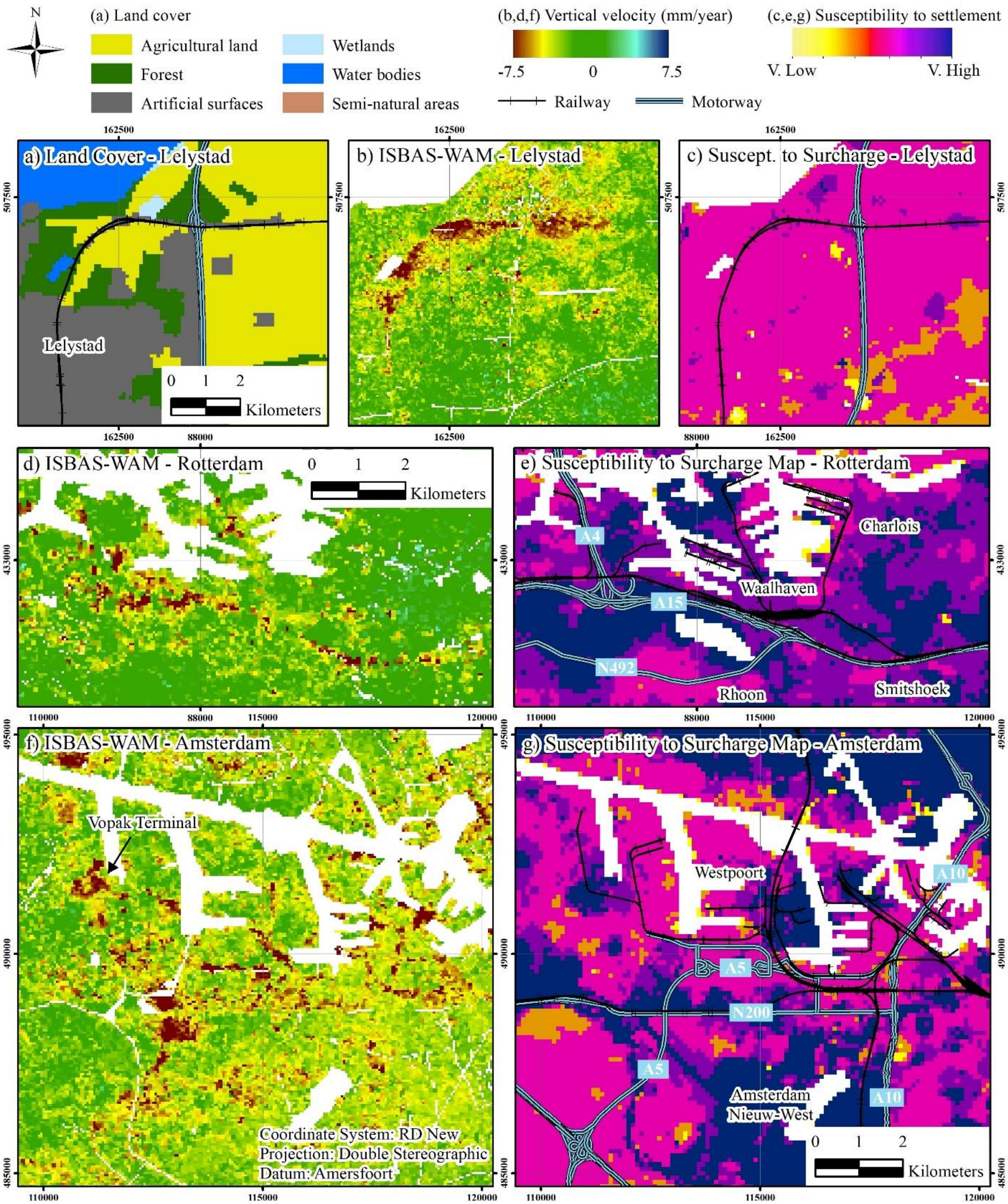

Figure 8. Infrastructure induced settlement: (a) CORINE Land Cover inventory (European Environment Agency, 2012) and transport infrastructure, (b) ISBAS-WAM vertical velocities (mm/year) and (c) susceptibility to surcharge map (De Lange *et al.*, 2012; Climate Impact Atlas, 2019) and transport infrastructure at Lelystad. (d) ISBAS-WAM

vertical velocities (mm/year) and (e) susceptibility to surcharge map (De Lange *et al.*, 2012; Climate Impact Atlas, 2019) and transport infrastructure at Rotterdam. (f) ISBAS-WAM vertical velocities (mm/year) and (g) susceptibility to surcharge map (De Lange *et al.*, 2012; Climate Impact Atlas, 2019) and transport infrastructure at Amsterdam. European Environment Agency © 2012, Climate Impact Atlas © 2019.

The longest near-continuous stretch of settlement occurs along an 80 km stretch of the Betuweroute, between Gorinchem and Elst (Figure 9a,b). The Betuweroute is a major double track freight railway running from Rotterdam to Germany. The track is built on clay, peat, gravel and sandy soils of the Rhine-Meuse-Scheldt river delta, which is particularly susceptible to compaction and settlement. Along the entire route deformation occurs in areas less susceptible to settlement, in the area to the east of Gorinchem (Figure 6c; 9a,b). This section crosses the alluvial plain of the Rhine, which contains more clay and less peat layers than the area west of Gorinchem. In the western areas, between Gorinchem and Rotterdam, the Betuweroute was constructed with attention to the characteristically settlement-prone soils and less settlement is observed here. Conversely, residual settlement in the clay-dominated fluvial plane area has resulted in noticeable vertical movements. These may develop in unwanted differential settlements, especially where buried sand-filled river valleys are crossed.

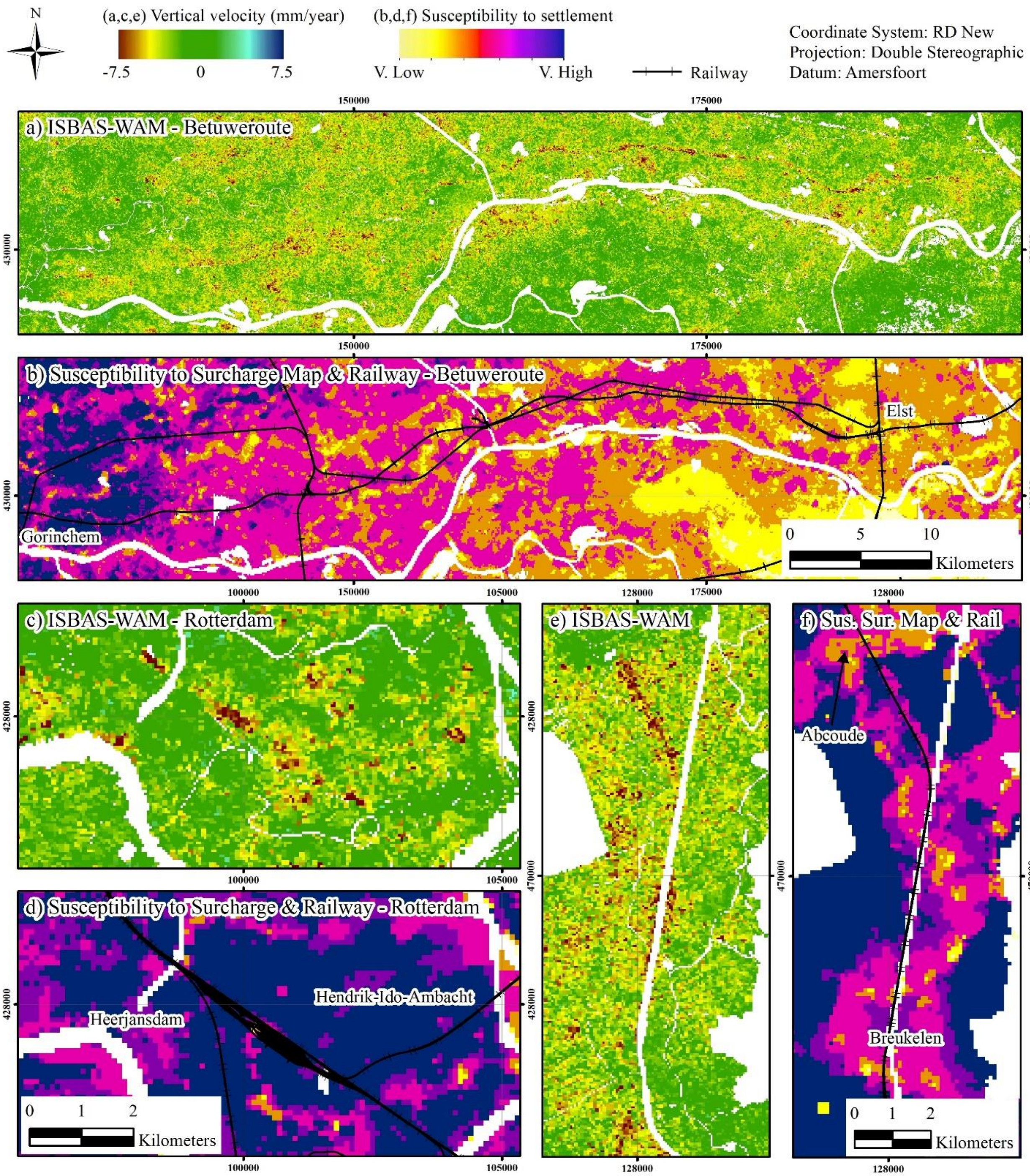

Figure 9. Settlement along rail routes: (a) ISBAS-WAM vertical velocities (mm/year) and (b) susceptibility to surcharge map (De Lange *et al.*, 2012; Climate Impact Atlas, 2019) of the Betuweroute. (c) ISBAS-WAM vertical velocities (mm/year) and (d) susceptibility to surcharge map (De Lange *et al.*, 2012; Climate Impact Atlas, 2019) of south east Rotterdam. (e) ISBAS-WAM vertical velocities (mm/year) and (f) susceptibility to surcharge map (De

Lange *et al.*, 2012; Climate Impact Atlas, 2019) on the route between Amsterdam and Utrecht. Climate Impact Atlas © 2019.

Full resolution PSI has previously been utilized for monitoring the structural health of rail infrastructure in the Netherlands, demonstrating the potential to offer a cost-effective alternative to in-situ measurements from survey trains, levelling or GPS (e.g. Peduto *et al.*, 2016; Chang *et al.*, 2017). Chang *et al.* (2017) used Radarsat-2 imagery (2010 – 2015) to detect differential motion over the entire rail network and, although the Sentinel-1 and Radarsat-2 analysis do not coincide in time, the spatial distribution of deformations is largely consistent. Whilst PSI returns measurements of the track itself, the ISBAS method is capable of ubiquitously measuring deformations in the surrounding environment which can provide additional insight into the cause of deformation; whether that be the repeated loading of the infrastructure by passing trains, soil compaction in the adjacent land or deeper processes such as salt mining.

There are also cases of deformation relating to other infrastructure (Figure 8d-g). In Rotterdam, residual settlement affects a 15 km stretch of the A15, which was recently widened (Figure 8d,e). The project was completed in early 2014 and ran significantly over budget due to doubts over the reliability of the foundations. In Amsterdam, a 9 km stretch of settlement is identified along the A5 motorway, which was opened in December 2012 (Figure 8f,g). A further example is at Vopak Terminal Amsterdam Westpoort, an oil storage terminal opened in 2011, where deformation correlates to an area of highest settlement susceptibility (Figure 8f,g).

5.3 Peat Oxidation

Subsidence occurs over areas of heathland located on elevated glacial deposits, including the Utrecht Hill Ridge, Hoge Veluwe National Park and perhaps most notably over the Sallandse Heuvelrug National Park (Figure 10). The Sallandse Heuvelrug national park is comprised of dry heathland and mixed deciduous-coniferous woodland. The heath landscape has changed substantially over the preceding 100 years due to anthropic influences; wet heath was dewatered and the top soil was removed to be utilized as fertilizer for agriculture, and dry heath was forested for wood production and to prevent erosion and sand-drifting. The park is now intensely managed to ensure degradation does not continue (Sallandse Heuvelrug, 2018).

Given these deformations are in areas of elevated topography (Figure 2a) and that dry heath is unaffected by variations in the phreatic surface (Sallandse Heuvelrug, 2018), deformation might be attributed to the erosion of the subsurface of coarse sand and the top layer of fine sand. Management practises such as the mowing and burning of heath might also contribute to this effect. Subsidence in these areas spatially correlates to the areas of heathland and these measurements, which almost entirely relate to intermittently coherent pixels, are reliable at the 5σ level (Figure 10c,f,i).

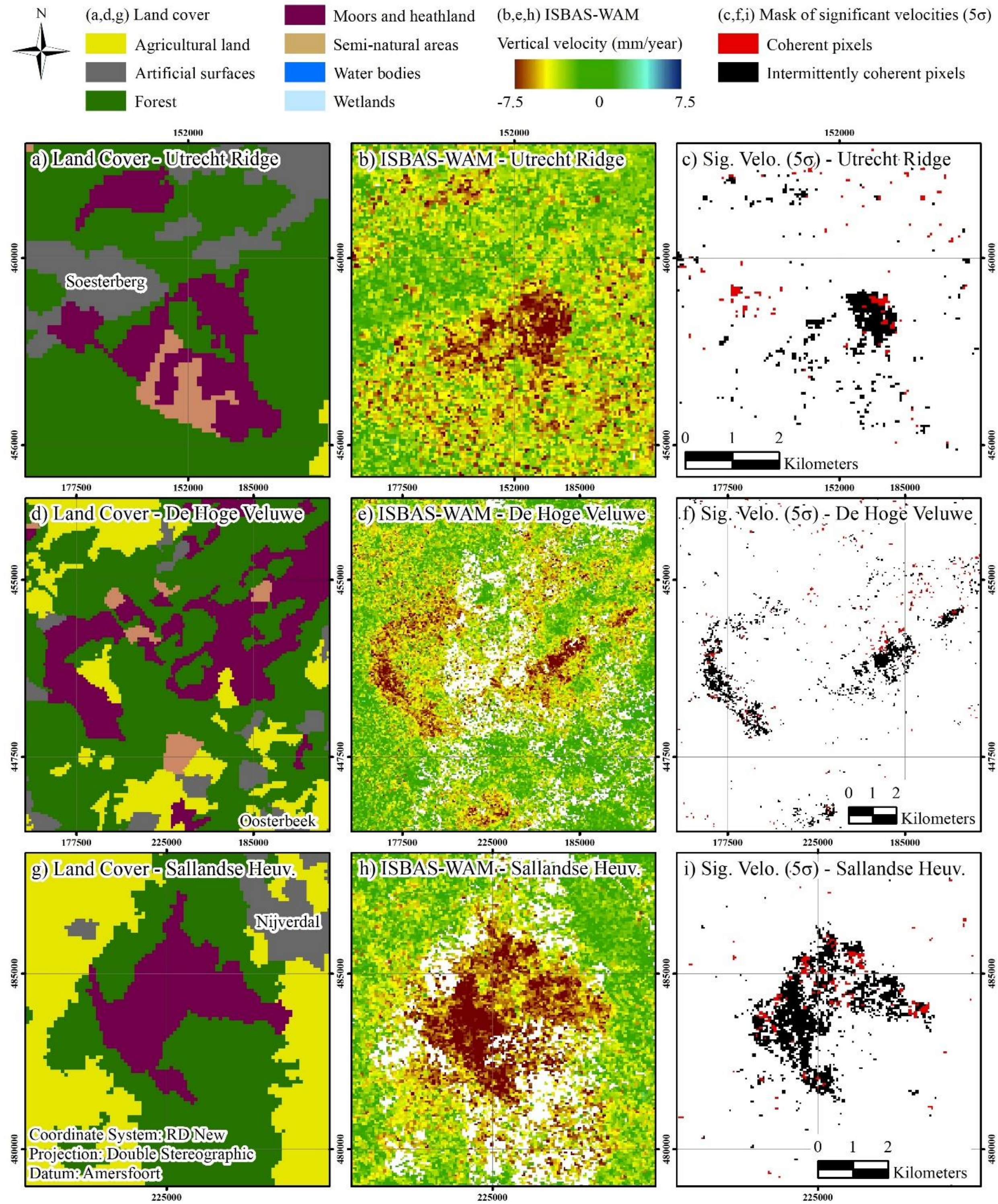

Figure 10. Heathland deformation: (a) CORINE Land Cover inventory (European Environment Agency, 2012), (b) ISBAS-WAM vertical velocities (mm/year) and (c) Mask of statistically significant deformations at 5σ (99.99994%) confidence level at Utrecht Hill Ridge. (d) CORINE Land Cover inventory (European Environment Agency, 2012), (e)

ISBAS-WAM vertical velocities (mm/year) and (f) Mask of statistically significant deformations at 5σ (99.99994%) confidence level at Hoge Veluwe National Park. (g) CORINE Land Cover inventory (European Environment Agency, 2012), (h) ISBAS-WAM vertical velocities (mm/year) and (i) Mask of statistically significant deformations at 5σ (99.99994%) confidence level at Sallandse Heuvelrug National Park. European Environment Agency © 2012.

5.4 Gas Extraction

The subsidence observed within the perimeter of the Groningen gas field in the north-east of the Netherlands (Figure 11) has been well documented (Ketelaar, 2009; de Waal *et al.*, 2015). Subsidence has previously been identified over the gas field by applying PSI to ERS and ENVISAT data, with rates in the range of 4–7 mm/year for the period 1992–2007 (Ketelaar, 2009). Slightly higher subsidence rates were calculated at some 7–8 mm/year as of 2015 (Pijpers & van der Laan, 2015; van Thienen-Visser & Breunese, 2015). However, production was restricted from 54 billion m^3 in 2013 to 27 billion m^3 in 2015/16 (Van 't Hof, 2017; van-Thienne-Visser *et al.*, 2018) because of a correlation established between rates of production and the frequency and magnitude of earthquakes (Bourne *et al.*, 2014). The estimated maximum predicted subsidence due to gas production up to 2050, as calculated in the 2015 Nederlandse Aardolie Maatschappij status report (NAM, 2015), is 45 cm (13.3 mm/year). The ISBAS-WAM reveals that the mean velocity within the perimeter the Groningen field for 2015–2017 is -4.07 ± 1.07 mm/year, which has a standard deviation of 2.03 mm. Figure 11d shows that much of this deformation is significant at the 5σ confidence level, even though located in a largely rural area where coherence is typically intermittent.

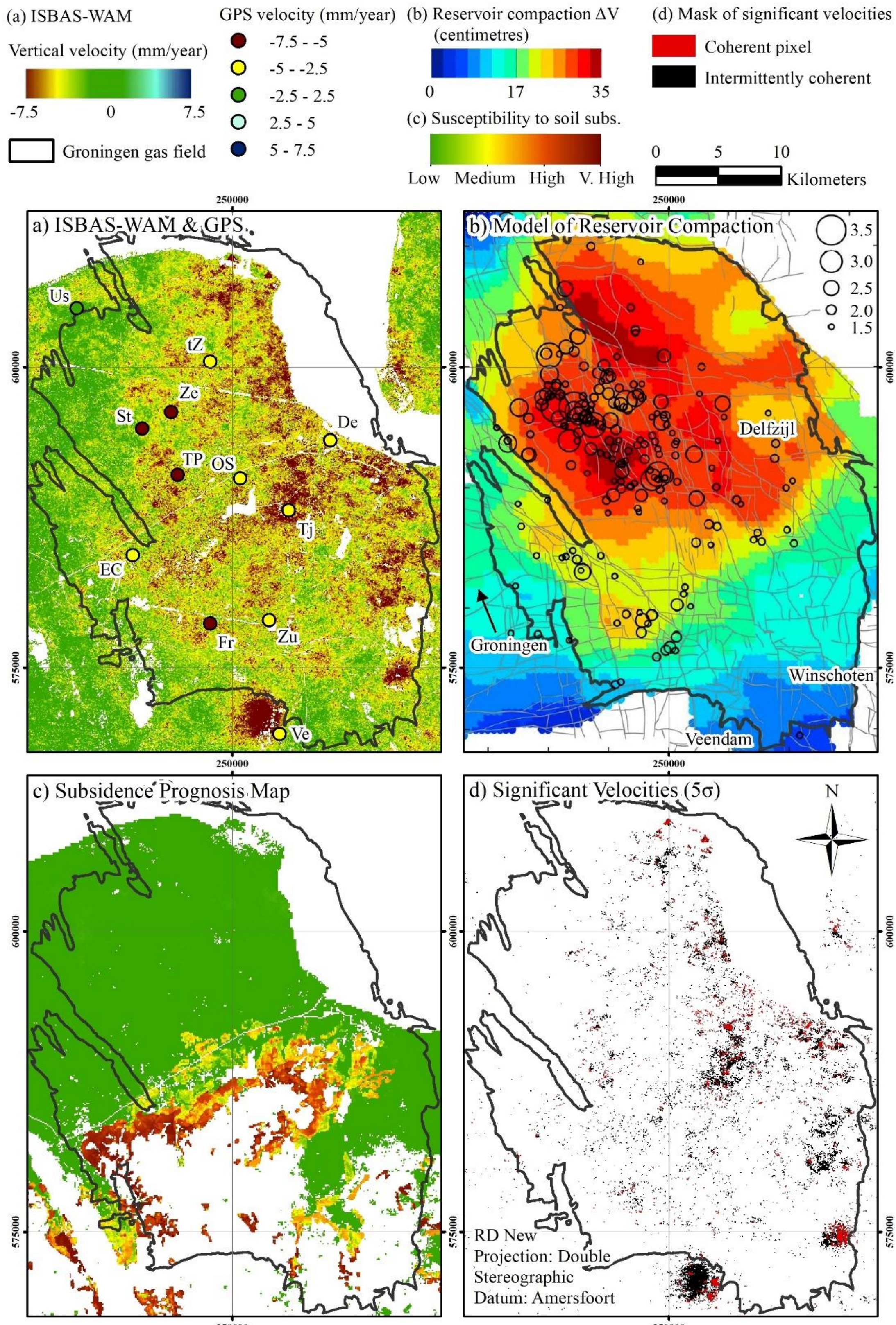

(a) ISBAS-WAM
Vertical velocity (mm/year)
-7.5
0
7.5
Groningen gas field
GPS velocity (mm/year)
-7.5 - -5
-5 - -2.5
-2.5 - 2.5
2.5 - 5
5 - 7.5
(b) Reservoir compaction ΔV (centimetres)
0
17
35
(c) Susceptibility to soil subs.
Low
Medium
High
V. High
(d) Mask of significant velocities
Coherent pixel
Intermittently coherent
0
5
10
Kilometers
a) ISBAS-WAM & GPS
Us
tZ
Ze
St
De
TP
OS
Tj
EC
Fr
Zu
Ve
b) Model of Reservoir Compaction
3.5
3.0
2.5
2.0
1.5
Delfzijl
Groningen
Winschoten
Veendam
c) Subsidence Prognosis Map
d) Significant Velocities (5σ)
N
RD New
Projection: Double
Stereographic
Datum: Amersfoort
250000
600000
575000

490

Figure 11. Subsidence over the Groningen field: (a) ISBAS-WAM vertical velocities, GPS velocities and Groningen gas field, (b) Model of reservoir compaction from 1960 to 2012, earthquake epicentres for $M_L \geq 1.5$ from 1995 to 2012 and Groningen gas field (adapted with permission from Bourne *et al.*, 2014), (c) Subsidence prognosis map and Groningen gas field (De Lange *et al.*, 2011; Climate Impact Atlas, 2019) and (d) Mask of statistically significant velocities at 5σ (99.99994%) confidence level and Groningen gas field. Climate Impact Atlas © 2019.

As an additional validation of the ISBAS-WAM, velocities from a sample of 12 GPS stations (NAM, 2018) for the same period of Sentinel-1 acquisitions over the Groningen area were compared to the corresponding nearest neighbour ISBAS velocity (Table 4; Figure 11a). The average GPS velocity was -4.44 ± 0.78 mm/year (at the 95% confidence level) while the average velocity for the corresponding locations in the ISBAS-WAM was -4.67 ± 1.18 mm/year, indicating that the two sets of deformation measurements concur. Estimated rates and patterns of deformation in the north Netherlands are complex given the contributions of deformation from shallow Holocene-related (i.e. peat) and deep sources (i.e. gas production) (Hanssen & Cuenca, 2012) and, despite agreement, it is still important to note that GPS and ISBAS measurements are not wholly comparable. GPS antennae are usually attached to built structures which are likely to have foundations that extend deeper than the Holocene layer. Therefore, any movement of such antenna is most likely associated with deeper sources of motion, such as gas production from Groningen. Conversely, the ISBAS measurements capture the combined deformation signal originating from both Holocene and deeper sources. An example of the incompatibility of the two measurements is at the Tjuchem station, located in an area of peat soil between Groningen and Delfzijl which is highly susceptibility to soil subsidence, where the

ISBAS measurement is over twice the magnitude of that measured by GPS (Table 4; Figure 11a,c). Further, the GPS measures the velocity of a point target, whereas the ISBAS velocity is representative of the sum of motions of a 90 x 90 m area, which can contain a mixture of hard and soft targets.

Table 4. Comparison of GPS and nearest neighbour ISBAS-WAM velocities over the Groningen gas field for the period 12th May 2015 – 13th May 2017. The locations of GPS monitoring stations are shown in Figure 11a.

GPS Monitoring Station	GPS Average Velocity (mm/year)	ISBAS-WAM Average Velocity (mm/year)	Error Difference (mm/year)
Delfzijl (De)	-4.05	-6.14	2.09
Ems Canal (EC)	-4.35	-2.61	-1.74
Froombosch (Fr)	-5.10	-3.93	-1.17
Over-shielded (OS)	-4.45	-4.40	-0.05
Stedum (St)	-5.15	-3.30	-1.85
Ten Post (TP)	-5.75	-4.75	-1.00
Tjuchem (Tj)	-4.00	-8.62	4.62
Usquert (Us)	-0.90	-1.40	0.50
Veendam (Ve)	-4.85	-5.30	0.45
‘t Zandt (tZ)	-4.75	-5.24	0.49
Zuiderveen (Zu)	-4.45	-6.12	1.67
Zeerijp (Ze)	-5.5	-4.25	-1.25
Mean	-4.44	-4.67	0.23
RMSE	-	-	1.82

5.5 Salt Mining

Subsidence in the north of the Netherlands also relates to underground salt mining. Two subsidence bowls coincide with salt mines in the Veendam concession, specifically within the bounds of the Veendam and Adolf van Nassau II & III license areas (Figure 12a). The maximum subsidence over Veendam between 1993 and 2004 was measured as 170 mm (on average corresponding to ~15 mm/year) by levelling and 155 mm (~14 mm/year) by PSI on ERS data (Humme, 2007). The Sentinel-1 analysis indicates subsidence in the region continued into 2015–2017, the majority of which occurs in a rural area and is predominantly characterised by intermittently coherent pixels with a high degree of confidence (5σ) (Figure 12b,c). A maximum rate of subsidence of -18.32 ± 0.96 mm/year and -18.06 ± 0.86 mm/year is observed over Veendam and Adolf van Nassau II & III respectively.

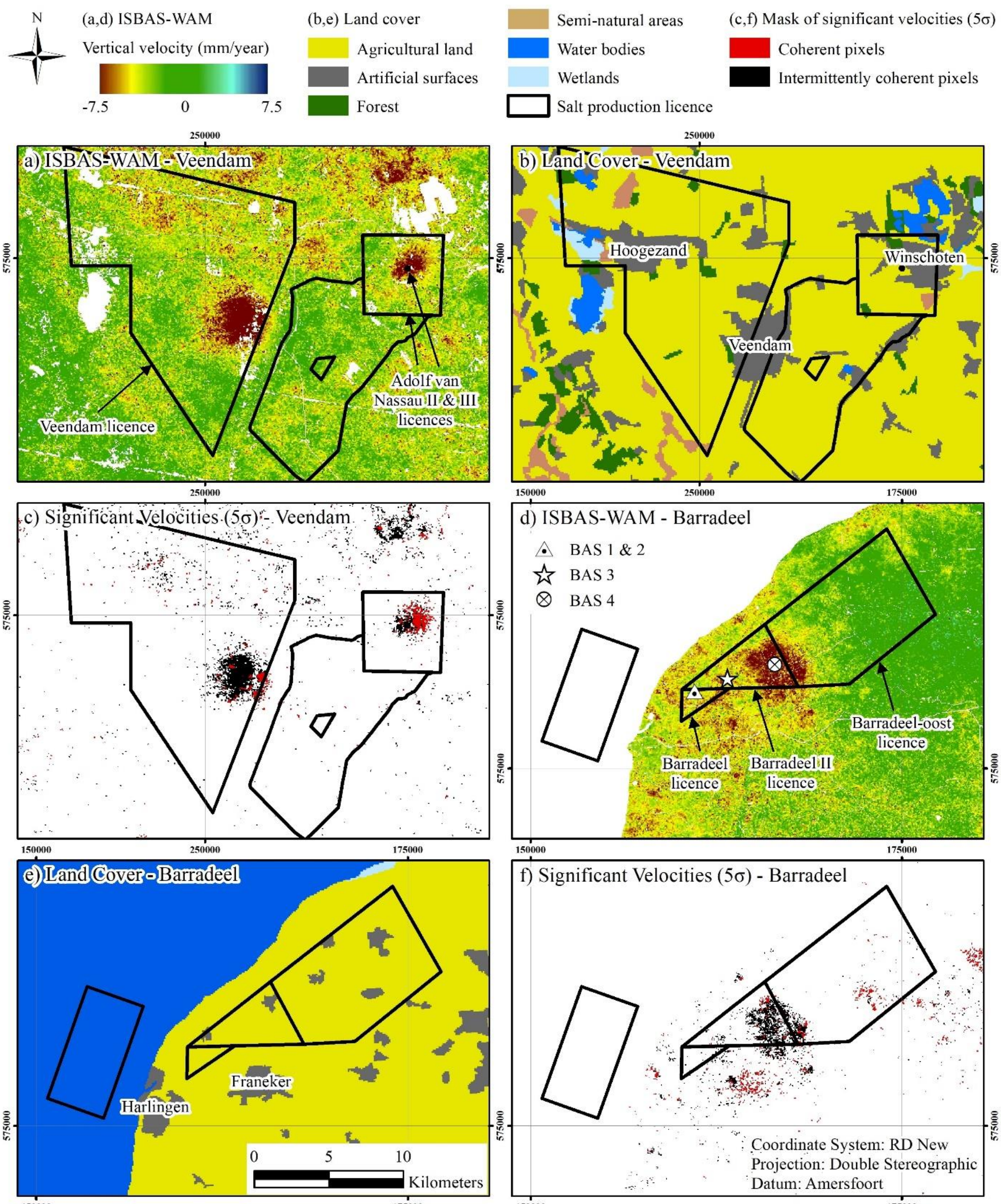

Figure 12. Subsidence attributed to salt mining in the north of the Netherlands: (a) ISBAS-WAM vertical velocities (mm/year), (b) CORINE Land Cover inventory (European Environment Agency, 2012) and (c) Mask of statistically significant deformations at 5σ (99.99994%) confidence level over the Veendam concession, Groningen. (d) ISBAS-

WAM vertical velocities (mm/year), (e) CORINE Land Cover inventory (European Environment Agency, 2012) and (f) Mask of statistically significant deformations at 5σ (99.99994%) confidence level over the Barradeel concession, Franeker. European Environment Agency © 2012.

Deformation also occurs in Friesland within the Barradeel II licence area, centred on borehole BAS-4 which has been utilized for solution mining since 2006 (Figure 12d). Subsidence reaches a maximum of -13.77 ± 1.42 mm/year and is characterised with a high degree of confidence (5σ) over agricultural fields (Figure 12e,f). Subsidence was previously identified over BAS-1 and BAS-2 using PSI in conjunction with ERS and ENVISAT data (Humme, 2007). BAS-1 is now utilized as a reserve cavern, while BAS-2 ceased operation in 2004. As expected, a well-defined subsidence bowl is no longer present over this area given that salt production has all but ceased. Some deformation is observed but this is more likely to be related to soil subsidence rather than deeper geological processes given that it is less spatially correlated than would be expected of a typical subsidence bowl overlying a salt mine.

5.6 Coal Mining

The largest resources of Dutch coal exist in the southern province of Limburg, which were exploited extensively until 1965. Long term extraction can result in subsidence following the collapse of mine galleries and groundwater pumping. Once abandoned, pumping regimes cease and uplift often occurs when pore pressure of the overburden increases as groundwater flows back to hydrostatic equilibrium (Bekendam & Pöttgens, 1995). Uplift (or heave) of up to approximately 5 mm/year is identified over the Roer Valley Rift System in the south east of the Netherlands (Figure 13). Surface heave has been previously identified between 1992–2009 using PSI, ranging from 1–8 mm/year and significantly correlated to rising groundwater following the cessation of pumping in the early 1990s (Cuenca *et al.,* 2013). Uplift over the course of the 1990s and 2000s was greatest around Geleen towards the western half of the mine concession and to a lesser extent in the east towards Brunssum. The ISBAS-WAM shows that this trend has reversed, with uplift now greater in the eastern part.

Uplift also occurs in the neighbouring Aachen coal district in Germany and the Belgian Campine Basin (Figure 13). In the Aachen district, greater rates of uplift of up to 11 mm/year occur, suggesting that the rates of groundwater rebound for the period May 2015 - May 2017 are greater in the Aachen district than in the Netherlands. The Belgian mines were closed between 1966 and 1992; however, no measurements of ground-water levels have been taken since closure (Vervoort & Declercq, 2017). Nonetheless, using ERS and ENVISAT data, Vervoort & Declercq (2017) identified residual subsidence in the west of the Campine Basin for a period of ~10 years after closure, whilst the uplift was found in the east in 1992, 4–5 years after closure. Surface uplift in Belgium is now of a greater magnitude in the west, up to 6 mm/year, indicating that groundwater levels are now rising faster in the west.

Large areas of subsidence are associated with the Rhineland lignite mining region, as also previously detected using PSI (Cuenca *et al.*, 2011; Hanssen & Cuenca, 2012). The subsidence within open cast mines corresponds to erosion of the surfaces due to extraction and the effects of dewatering programmes. Subsidence here is typically between -10 mm/year and -15 mm/year and deformation extends far beyond the extents of the mines due to groundwater pumping (Figure 13).

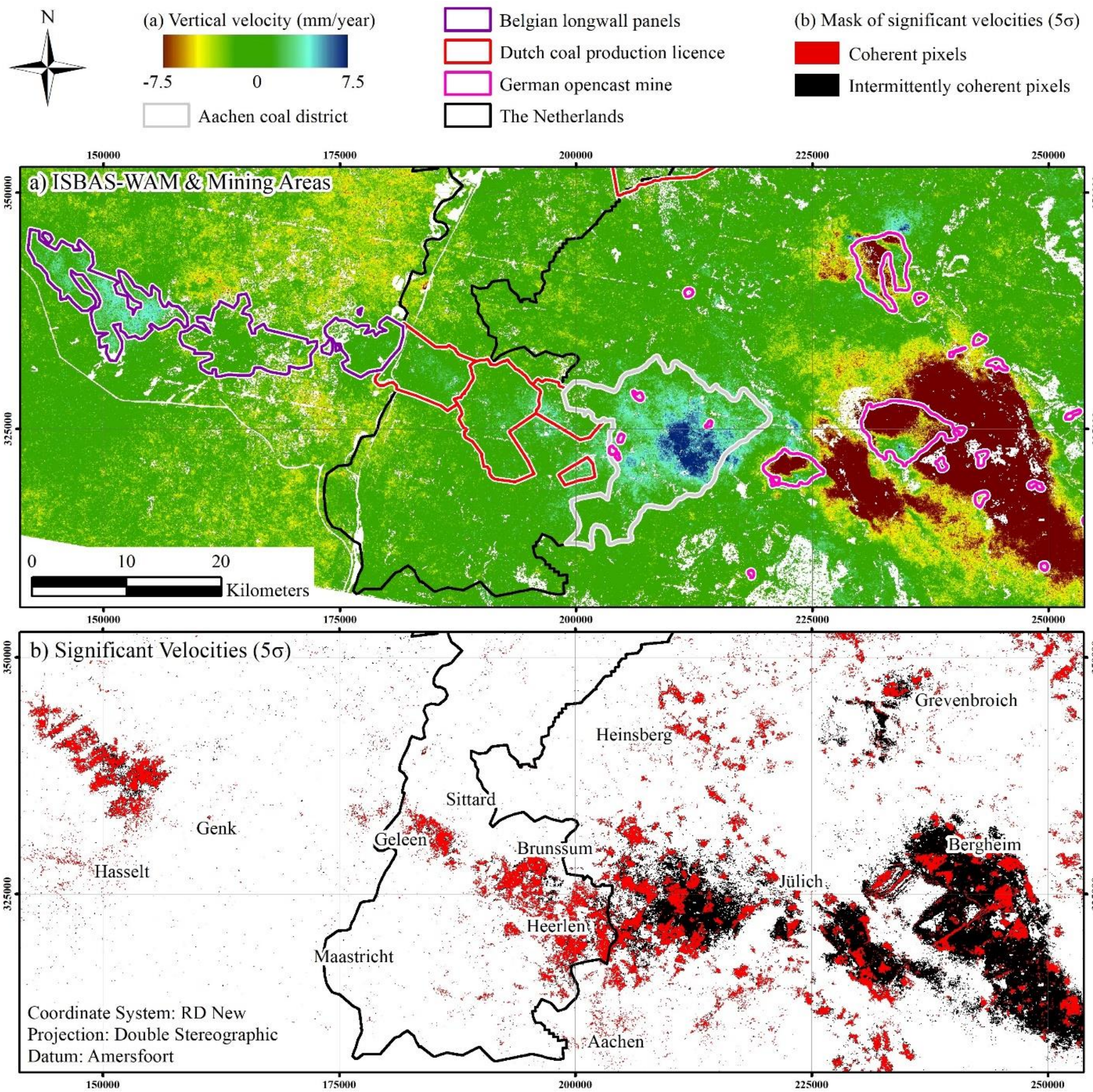

Figure 13. Mining related deformations covering Belgium, the Netherlands and Germany: (a) ISBAS-WAM vertical velocities (mm/year) and mining areas and (b) Mask of statistically significant deformations at 5σ (99.99994%) confidence level.

6. Operational Monitoring Outlook

Although InSAR is now a mature technology, it is still far less established in comparison to more conventional surveying techniques such as GPS-GNSS, total stations and levelling. Whilst Italy has had a national PSI database for several years (Costantini *et al.*, 2017), Copernicus has been the catalyst for other European countries, such as Norway, France, Denmark, Germany and the Netherlands (ESA, 2017; Oyen, 2017; NGU, 2019), to transition from ad hoc surveys into systematic operational nationwide monitoring. The results presented here demonstrate that the processing flow has the potential to be scaled for methodical production. However, such production is expensive in relation to storage, memory and computational power and presents a variety of challenges with respect to tasking capability and big data. This challenge is illustrated by the calculation of the feasibility of a single geometry European-wide product, which highlights the substantial quantity of imagery required, volume of intermediate data to be produced and the number of measurements which will be computed (Table 5; Figure 14). Furthermore, to generate the absolute vertical and horizontal components of motion, solutions from both ascending and descending geometries are required, and to determine time-series for each pixel, residual phase components need to be unwrapped, which are significant additional computational loads.

Table 5. Data requirements for an average velocity European deformation map for a two-year period using Sentinel-1 data.

Statistic	**Ascending Europe-WAM**
Land Surface Area (Km^2)	4 914 364
Nº of Frames	293
Nº of Images	35160
Vol. of Imagery (Terabytes)	141
Nº Interferometric Stacks	440
Vol. of Processed Interferometric Stacks (Terabytes)	396
Cumulative Processing Time (Days)	1320
Modelled Nº of Solutions	1 706 145 321
Modelled Density (Solutions/km^2)	347
Modelled Ground Coverage (%)	87
Modelled Mean Standard Error (mm/year)	1.10

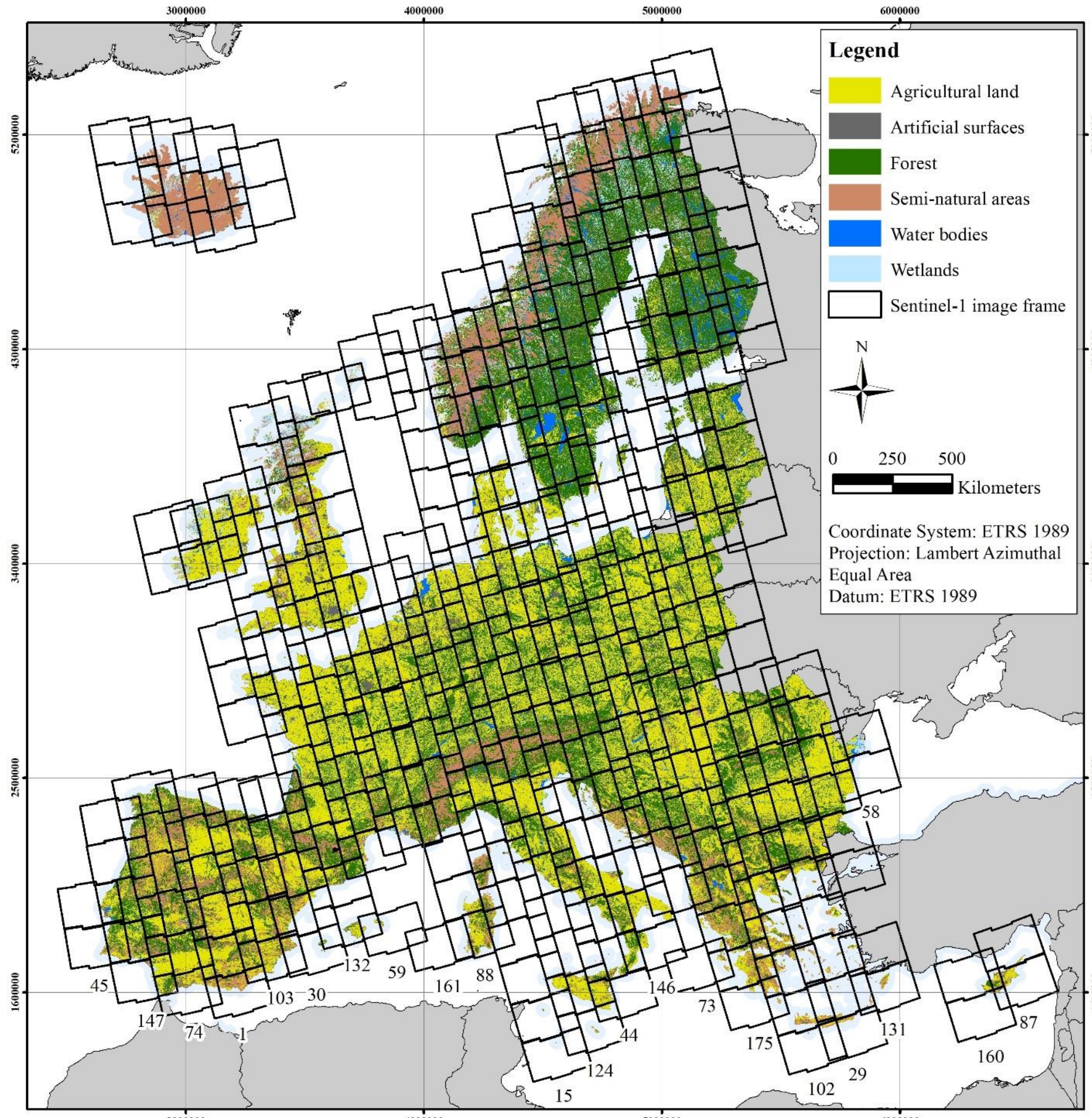

Figure 14. Footprints of Sentinel-1 frames required to cover mainland Europe, encompassing the European Economic Area, Switzerland and the western Balkan countries, in an ascending geometry and CORINE Land Cover inventory (European Environment Agency, 2012). Labels define each relative orbital track. European Environment Agency © 2012.

The migration of the required software onto a Cloud computing environment provides a viable solution to negate volume and efficiency issues and have already demonstrated the potential to deliver efficient multi-user services for InSAR (e.g. De Luca *et al*., 2017). Central to efficient processing is automation; computation via the ISBAS method currently requires relatively minimal operator interaction, such that only relatively minor modifications would be required to fulfil this objective. Automated processing in combination with regular, near global, systematic acquisitions from the Sentinel-1 mission would be a potentially unprecedented resource of 'big' InSAR data which could be transformational for the downstream EO community.

The quality of such a volume of autonomously derived data is central to ensure deformation information is reliable. In this study it has been demonstrated that on average millimetre precision was achieved for nearly 20 million ISBAS solutions. The Netherlands has an abundance of geodetic infrastructure (e.g. gravimeter network, GNSS reference stations, Normaal Amsterdams Peil height reference system, regular national-scale airborne LiDAR) for which to corroborate spaceborne InSAR measurements. However, elsewhere in Europe, the availability of such accurate and precise ground truth data with sufficient spatial and temporal sampling is less common. Despite not performing any absolute referencing, ISBAS measurements concur with independent GPS data over Groningen. This indicates that reliable results can be achieved without referencing, which bodes well for forthcoming products in countries where geodetic ground truth is unavailable.

Future operational services need to be a multi-disciplinary undertaking, where InSAR specialists work alongside engineers, geologists, geophysicists and alike to combine InSAR datasets with ancillary information, such as lithological maps, land cover/use, DEMs, spatial development data and landslide inventories, to produce individual application-based products where deformations are evaluated and interpreted by geologists. For example, by combining information on the spatial distribution and severity of recorded infrastructure damages with concurrent satellite-derived deformation measurements, an empirical cause-effect relationship can be established and validated to produce damage forecasting models (e.g. Peduto *et al.*, 2018). Determining subsidence and settlement risk is a difficult and complex task that technical and scientific communities responsible for land-use planning and urban management rely upon (Peduto *et al.*, 2017). Such accurate risk and vulnerability information on a continental scale have enormous potential for providing information on potential geohazards.

7. Conclusion

The Netherlands has been subject to a multitude of initial studies that have highlighted the potential of InSAR to make monitoring strategies more cost-effective and efficient (e.g. Dentz *et al.*, 2006; Dheenathayalan *et al.*, 2011; Hopman *et al.*, 2013; Peduto *et al.*, 2016; Chang *et al.*, 2017). This study demonstrates that, by utilizing large volumes of Sentinel-1 C-Band SAR data, national scale ground motion maps are now achievable following the establishment of the Copernicus programme. The ISBAS-WAM was produced from a total of 435 Sentinel-1 images through the computation of average velocities from six individual interferometric stacks, which were subsequently combined into a seamless mosaic. By utilizing the ISBAS method, 94% of the land surface area was surveyed, achieving unprecedented coverage solely using InSAR. The retrieval of low-resolution measurements over soft surfaces was crucial in achieving this, due the dominance of non-urban land cover in the Netherlands. The resulting ubiquitous spatial coverage aided the delineation and quantification of deformation features. A statistical analysis of velocities demonstrates that intermittently coherent measurements can provide reliable (5σ), additional deformation information outside of urban areas. The main causes of deformation were attributed to compressible soils, infrastructure settlement, peat oxidation, gas production, salt mining and underground and opencast mining. Across the mosaic, the spatial distribution of deformation concurs with independent sources of data, such as previous PSI-based deformation maps (e.g. Cuenca *et al.*, 2011; Hanssen & Cuenca, 2012; Chang *et al.*, 2017; Oyen, 2017), models of subsidence and settlement susceptibility (De Lange *et al.*, 2011; De Lange *et al.*, 2012; Climate Impact Atlas, 2019), and quantitatively with GPS measurements over the Groningen gas field.

Nationwide deformation products are a powerful and cost-effective tool for informing risk mitigation strategies against geological issues resulting from natural and anthropogenic phenomena. Although cost estimations related to ground motion are not straightforward, damage associated with deformation in the Netherlands was estimated at over €3.5 billion in 2006 (Erkens *et al.,* 2015). Attempts to mitigate this cost rely upon early identification and implementation of intermediary measures to prevent damage becoming considerably more serious. Examples have shown there can be an order of magnitude difference between reaching an asset in time to conduct repairs and having to undertake emergency works (Environment Agency, 2018). The delineation and quantification of subsidence at broader spatial scales is, therefore, crucial for the sustainable management of the environment and Earth resources (van der Meulen *et al.*, 2013) and is fundamentally embedded within Dutch government policy (Erkens *et al.,* 2015).

Dense survey data of ground motions is vital to better comprehend the impact of ground heterogeneities (Ngan-Tillard *et al.*, 2010). The ISBAS-WAM, which uniquely has near complete ground coverage, can be analysed to readily screen and identify affected regions, which may require more detailed local-scale follow-up geological and geotechnical investigation. The product provides critical information on Earth-structure interactions which can be utilized to inform the location, design, construction, operation and maintenance of infrastructure (e.g. Peduto *et al.*, 2016). Such data can also be of use for optimising renovations to subsurface utilities, climate change adaption, as well as for insurance, engineering, road and rail companies, and local authorities, amongst others.

The only practical approach from which timely, reliable, systematic geohazard information can be derived throughout Europe is through the use of remote sensing. In this regard, the product generated over the Netherlands clearly demonstrates the potential of the ISBAS method for providing precise deformation information on that scale. However, it is clear that the generation of regularly updated national or European products will not be simple due to computational challenges related to scaling-up the processing and the characteristics of the environment. In relation to computing, developing a systematic semi-automated production platform requires algorithmic, data management and product development challenges to be addressed. From an EO perspective, deriving velocities over complex topography (e.g. fjords and mountains) and non-urban areas – comprising 94% of the land cover in Europe (European Environment Agency, 2012) – is challenging. Areas characterised by highly variable topography will require careful assimilation of results from multiple geometries; nonetheless, as demonstrated here, the ISBAS method offers an effective algorithmic solution for reliably monitoring deformation over vegetated environments with a high degree of confidence.

Acknowledgements:

The work conducted here was funded by the GeoEnergy Research Centre and Geomatic Ventures Limited. Sentinel-1 SAR data was sourced from the Copernicus Open Access Hub (https://scihub.copernicus.eu/dhus/#/home); mining and oil and gas data from NLOG (http://www.nlog.nl/en/files-interactive-map); topographic map, rail and roads from PDOK (https://www.pdok.nl/en/producten/pdok-services/overzicht-urls); landscape types and the subsidence and settlement susceptibility maps from the Climate Impact Atlas (http://www.klimaateffectatlas.nl/en/); and GPS data from NAM (https://nam-feitenencijfers.data-app.nl/). Belgian longwall panels and the Aachen coal district were digitized from publicly available sources. The authors would like to acknowledge the anonymous reviewers who helped to improve the quality of the manuscript.

Declarations of interest: none.

References:

1. Adam, N., Parizzi, A., Eineder, M. and Crosetto, M., 2009. Practical persistent scatterer processing validation in the course of the Terrafirma project. *Journal of Applied Geophysics*, *69*(1), pp.59-65. DOI: 10.1016/j.jappgeo.2009.07.002
2. Adam, N., Gonzalez, F.R., Parizzi, A. and Liebhart, W., 2011. Wide area persistent scatterer interferometry. In *Geoscience and Remote Sensing Symposium (IGARSS), 2011 IEEE International* (pp. 1481-1484). IEEE. DOI: 10.1109/IGARSS.2011.6049347
3. Bayer, B., Simoni, A., Schmidt, D. and Bertello, L., 2017. Using advanced InSAR techniques to monitor landslide deformations induced by tunneling in the Northern Apennines, Italy. *Engineering Geology*, *226*, pp.20-32. DOI: 10.1016/j.enggeo.2017.03.026
4. Bekendam, R.F. and Pöttgens, J.J., 1995. Ground movements over the coal mines of southern Limburg, The Netherlands, and their relation to rising mine waters. *Land Subsidence (Proc. Fifth Int. Symp. On Land Subsidence, The Hague, October 1995)*. IAHS Publ. no. 234., pp.3-12.
5. Berardino, P., Fornaro, G., Lanari, R. and Sansosti, E., 2002. A new algorithm for surface deformation monitoring based on small baseline differential SAR interferograms. *IEEE*

Transactions on Geoscience and Remote Sensing, *40*(11), pp.2375-2383. DOI: 10.1109/TGRS.2002.803792

6. Bonì, R., Herrera, G., Meisina, C., Notti, D., Béjar-Pizarro, M., Zucca, F., González, P.J., Palano, M., Tomás, R., Fernández, J. and Fernández-Merodo, J.A., 2015. Twenty-year advanced DInSAR analysis of severe land subsidence: The Alto Guadalentín Basin (Spain) case study. *Engineering Geology, 198*, pp.40-52. DOI: 10.1016/j.enggeo.2015.08.014
7. Bourne, S.J., Oates, S.J., Elk, J.V. and Doornhof, D., 2014. A seismological model for earthquakes induced by fluid extraction from a subsurface reservoir. *Journal of Geophysical Research: Solid Earth*, *119*(12), pp.8991-9015. DOI: 10.1002/2014JB011663.
8. Capes, R., 2012, September. PanGeo: Enabling Access to Geological Information in Support of GMES. In *1st EAGE/GRSG Remote Sensing Workshop*. DOI: 10.3997/2214-4609.20143281.
9. Castelletto, N., Ferronato, M., Gambolati, G., Janna, C., Marzorati, D. and Teatini, P., 2013. Can natural fluid pore pressure be safely exceeded in storing gas underground?. *Engineering Geology, 153*, pp.35-44. DOI: 10.1016/j.enggeo.2012.11.008
10. Chang, L., Dollevoet, R.P. and Hanssen, R.F., 2017. Nationwide Railway Monitoring Using Satellite SAR Interferometry. *IEEE Journal of Selected Topics in Applied Earth Observations and Remote Sensing*, *10*(2), pp.596-604. DOI: 10.1109/JSTARS.2016.2584783
11. Chaussard, E., Amelung, F., Abidin, H. and Hong, S.H., 2013. Sinking cities in Indonesia: ALOS PALSAR detects rapid subsidence due to groundwater and gas extraction. *Remote Sensing of Environment*, *128*, pp.150-161. DOI: 10.1016/j.rse.2012.10.015

12. Chaussard, E., Wdowinski, S., Cabral-Cano, E. and Amelung, F., 2014. Land subsidence in central Mexico detected by ALOS InSAR time-series. *Remote sensing of Environment*, 140, pp.94-106. DOI:10.1016/j.rse.2013.08.038
13. Climate Impact Atlas, 2019. *Soil Subsidence*. Available at: <http://www.klimaateffectatlas.nl/en/story-map-drought> [Accessed 20 March 2018].
14. Colesanti, C., Ferretti, A., Prati, C. and Rocca, F., 2003. Monitoring landslides and tectonic motions with the Permanent Scatterers Technique. *Engineering Geology, 68*(1-2), pp.3-14. DOI: 10.1016/S0013-7952(02)00195-3
15. European Environment Agency, 2012. *CORINE Land Cover 2012*. Available at: <https://land.copernicus.eu/pan-european/corine-land-cover/clc-2012/view> [Accessed 21 January 2018].
16. Costantini, M., Ferretti, A., Minati, F., Falco, S., Trillo, F., Colombo, D., Novali, F., Malvarosa, F., Mammone, C., Vecchioli, F. and Rucci, A., 2017. Analysis of surface deformations over the whole Italian territory by interferometric processing of ERS, Envisat and COSMO-SkyMed radar data. *Remote Sensing of Environment*, *202*, pp.250-275. DOI: 10.1016/j.rse.2017.07.017.
17. Crosetto, M., Monserrat, O., Iglesias, R. and Crippa, B., 2010. Persistent scatterer interferometry. *Photogrammetric Engineering & Remote Sensing*, *76*(9), pp.1061-1069. DOI: 10.14358/PERS.76.9.1061
18. Cuenca, M.C., Hanssen, R., 2008. Subsidence due to peat decomposition in The Netherlands, kinematic observations from radar interferometry. In: *Proceedings Fringe 2007 Workshop, Frascati, Italy Workshop* (pp. 1-6).

19. Cuenca, M.C., Hanssen, R., Hooper, A. and Arikan, M., 2011. Surface deformation of the whole Netherlands after PSI analysis. In *Proceedings Fringe 2011 Workshop, Frascati, Italy* (pp. 19-23).
20. Cuenca, M.C., Hooper, A.J. and Hanssen, R.F., 2013. Surface deformation induced by water influx in the abandoned coal mines in Limburg, The Netherlands observed by satellite radar interferometry. *Journal of Applied Geophysics, 88*, pp.1-11. DOI: 10.1016/j.jappgeo.2012.10.003
21. De Lange, G., Oosthoek, J.T., and Gunnink, J.L.T. 2011. *Maaivelddalings prognose voor 2050, onderdeel van de scenarios van het Deltamodel, in Deltascenario's, report 1205747-000-veb- 0005 (in Dutch). Technical report*. Deltares, Utrecht.
22. De Lange, G., Bakr, M., Gunnink, J. L., and Huisman, D.J. 2012. A Predictive Map of Compression- Sensitivity of the Dutch Archaeological Soil Archive. *Conservation and Management of Archaeological Sites*, *14*(1-4), pp.284-293. DOI: 10.1179/1350503312Z.00000000024
23. Dentz, F., van Halderen, L., Possel, B., Esfahany, S.S., Slobbe, C. and Wortel, T., 2006. *On the Potential of Satellite Radar Interferometry for Monitoring Dikes of the Netherlands*. [pdf] Geomatics, Faculty of Aerospace Engineering, Delft University of Technology. Available at: <https://d1rkab7tlqy5f1.cloudfront.net/TUDelft/Onderwijs/Opleidingen/Master/MSc_Geomatics/2006_Geomatics_Synthesis_Project.pdf> [Accessed 21 January 2017].
24. De Luca, C., Zinno, I., Manunta, M., Lanari, R. and Casu, F., 2017. Large areas surface deformation analysis through a cloud computing P-SBAS approach for massive

processing of DInSAR time series. *Remote Sensing of Environment*, *202*, pp.3-17. DOI: 10.1016/j.rse.2017.05.022.

25. De Mulder, E.F.J., 1994. The Netherlands without engineering geology: No lands. *Engineering Geology, 37*(1), pp.5-14. DOI: 10.1016/0013-7952(94)90077-9
26. Dheenathayalan, P., Cuenca, M.C. and Hanssen, R., 2011. Different approaches for PSI target characterization for monitoring urban infrastructure. In *8th International Workshop on Advances in the Science and Applications of SAR Interferometry. Frascati (Italy).*
27. Environment Agency, 2018. *Space Derived Condition Assessment tool for Critical National Infrastructure Structural Risk Management*. (Personal Communication, Great George Street, London, 19th November 2018).
28. Erkens, G., Bucx, T., Dam, R., De Lange, G. and Lambert, J., 2015. Sinking coastal cities. *Proceedings of the International Association of Hydrological Sciences*, *372*, pp.189-198. DOI: doi:10.5194/piahs-372-189-2015
29. Erkens, G., van der Meulen, M.J. and Middelkoop, H., 2016. Double trouble: subsidence and CO 2 respiration due to 1,000 years of Dutch coastal peatlands cultivation. *Hydrogeology Journal*, *24*(3), pp.551-568. DOI: 10.1007/s10040-016-1380-4
30. ESA, 2017. *Fringe 2017 Workshop: Advances in the Science and Applications of SAR Interferometry and Sentinel-1 InSAR.* [pdf] Aalto University, Helsinki, Finland. Available at:<http://fringe.esa.int/files/Fringe2017_Abstract_Book_FINAL.pdf> [Accessed 24th November 2018]

31. Ferretti, A., Fumagalli, A., Novali, F., Prati, C., Rocca, F. and Rucci, A., 2011. A new algorithm for processing interferometric data-stacks: SqueeSAR. *IEEE Transactions on Geoscience and Remote Sensing, 49*(9), pp.3460-3470. DOI: 10.1109/TGRS.2011.2124465

32. Ferretti, A., Prati, C. and Rocca, F., 2001. Permanent scatterers in SAR interferometry. *IEEE Transactions on Geoscience and Remote Sensing, 39*(1), pp.8-20. DOI: 10.1109/36.898661

33. Gee, D., Bateson, L., Sowter, A., Grebby, S., Novellino, A., Cigna, F., Marsh, S., Banton, C. and Wyatt, L., 2017. Ground motion in areas of abandoned mining: application of the Intermittent SBAS (ISBAS) to the Northumberland and Durham Coalfield, UK. *Geosciences*, *7*(3), p.85. DOI: 10.3390/geosciences7030085

34. Gee, D., Sowter, A., Novellino, A., Marsh, S. and Gluyas, J., 2016. Monitoring land motion due to natural gas extraction: Validation of the Intermittent SBAS (ISBAS) DInSAR algorithm over gas fields of North Holland, the Netherlands. *Marine and Petroleum Geology*, 77, pp.1338-1354. DOI: 10.1016/j.marpetgeo.2016.08.014

35. Gruijters, S. and van der Krogt, R., 2013. TerraFirma and SubCoast: using satellite data for flood related issues and ground subsidence. In *EGU General Assembly Conference Abstracts* (Vol. 15).

36. Hanssen, R.F. and Cuenca, M.C., 2012. Absolute Wide Scale Subsidence Map of The Netherlands. European Commission Research Executive Agency: Brussels, Belgium; October 2012. 27p. Available at: <http://www.subcoast.eu/alfresco/d/d/workspace/SpacesStore/2be57ae8-a69c-48da-b06c-816a3f85e36d/D3.2.1%20Absolute%20Nation%20Wide%20Map.pdf> [Accessed 17th June 2018].

37. Hooper, A., 2008. A multi-temporal InSAR method incorporating both persistent scatterer and small baseline approaches. *Geophysical Research Letters, 35*(16). DOI: 10.1029/2008GL034654

38. Hooper, A., Zebker, H., Segall, P. and Kampes, B., 2004. A new method for measuring deformation on volcanoes and other natural terrains using InSAR persistent scatterers. *Geophysical research letters*, *31*(23). L23611. DOI: 10.1029/2004GL021737.

39. Hopman, V., de Lange, G., Vonhögen, L., Kruiver, P., van Leijen, F., and Ianoschi, R., 2013. Report on pilot service Rhine-Meuse Delta, Subcoast Deliverable D3.2.3. Available at:<http://www.subcoast.eu/alfresco/d/d/workspace/SpacesStore/d7ea539e-ae29-460b-be82-50ca2b2ab011/D3.2.3%20SubCoast%20report%20Rhine%20Meuse%20Delta_final.pdf> [Accessed 24th July 2018].

40. Humme, A.J.M., 2007. *Point density optimization for SAR interferometry: a study tested on salt mine areas* (Doctoral dissertation, MS thesis, Department of Earth Observation and Space Systems, Faculty of Aerospace Engineering, (Delft University of Technology, Delft, The Netherlands 2007)).

41. Ketelaar, V.B.H., 2009. *Satellite Radar Interferometry: Subsidence Monitoring Techniques*, Remote Sens. and Digital Image Processing, Vol. 13, 243 pp., Springer.

42. Lu, Z. and Kwoun, O.I., 2008. Radarsat-1 and ERS InSAR analysis over southeastern coastal Louisiana: Implications for mapping water-level changes beneath swamp forests. *IEEE Transactions on Geoscience and Remote Sensing*, *46*(8), pp.2167-2184. DOI: 10.1109/TGRS.2008.917271

43. Marshall, C., Large, D.J., Athab, A., Evers, S.L., Sowter, A., Marsh, S. and Sjögersten, S., 2018. Monitoring tropical peat related settlement using ISBAS InSAR, Kuala Lumpur International Airport (KLIA). *Engineering Geology*, *244*, pp.57-65. DOI: 10.1016/j.enggeo.2018.07.015

44. NAM, 2015. *Subsidence by natural gas extraction. NAM fields in Gronigen, Frieslands and the North of Drenthe: Status report 2015 and Prognosis to the year 2080*. Nederlandse Aardolie Maatschappij, Assen, The Netherlands. Available at:< http://www.commissiebodemdaling.nl/files/Status%20rapport%202015-final.pdf>

45. NAM, 2018. *Land Subsidence GPS Measurements*. [online] Available at:<https://nam-feitenencijfers.data-app.nl/embed/component/?id=Charts/bodemdaling/gps-metingen> [Accessed 27th July 2018].

46. Ngan-Tillard, D., Venmans, A. and Slob, E., 2010. Total engineering geology approach applied to motorway construction and widening in the Netherlands: Part I: A pragmatic approach. *Engineering Geology, 114*(3-4), pp.164-170. DOI: 10.1016/j.enggeo.2010.04.013

47. NGU, 2019. *InSAR Norway*. Geological Survey of Norway. Available at:< https://insar.ngu.no/> [Accessed 4th February 2019].

48. Oyen, A., 2017. *Towards an InSAR Based Nationwide Monitoring Strategy in the Netherlands*. Rijkswaterstaat (Ministry of Infrastructure and the Environment), the Netherlands. Available at: < http://fringe.esa.int/files/presentation526.pdf> [Accessed 21 January 2018].

49. Peduto, D., Elia, F. and Montuori, R., 2018. Probabilistic analysis of settlement-induced damage to bridges in the city of Amsterdam (The Netherlands). *Transportation Geotechnics, 14*, pp.169-182. DOI: 10.1016/j.trgeo.2018.01.002

50. Peduto, D., Huber, M., Speranza, G., van Ruijven, J. and Cascini, L., 2016. DInSAR data assimilation for settlement prediction: case study of a railway embankment in the Netherlands. *Canadian Geotechnical Journal, 54*(4), pp.502-517. DOI: 10.1139/cgj-2016-0425

51. Peduto, D., Nicodemo, G., Maccabiani, J. and Ferlisi, S., 2017. Multi-scale analysis of settlement-induced building damage using damage surveys and DInSAR data: A case study in The Netherlands. *Engineering Geology, 218*, pp.117-133. DOI: 10.1016/j.enggeo.2016.12.018

52. Pijpers, F. and van der Laan. D. J., 2015. Phase 1 update May 2015: trend changes in ground subsidence in Groningen, Statistics Netherlands Scientific paper, CBS, 14 pp.

53. Rohmer, J., Loschetter, A., Raucoules, D., De Michele, M., Raffard, D. and Le Gallo, Y., 2015. Revealing the surface deformation induced by deep CO2 injection in vegetated/agricultural areas: The combination of corner-reflectors, reservoir simulations and spatio-temporal statistics. *Engineering Geology, 197*, pp.188-197. DOI: 10.1016/j.enggeo.2015.08.005

54. Sallandse Heuvelrug, 2018. *About the area.* Nationaal Park De Sallandse Heuvelrug. Available at:< http://www.sallandseheuvelrug.nl/over-het-park> [Accessed 24th July 2018].

55. Sowter, A., Amat, M.B.C., Cigna, F., Marsh, S., Athab, A. and Alshammari, L., 2016. Mexico City land subsidence in 2014–2015 with Sentinel-1 IW TOPS: Results using the

Intermittent SBAS (ISBAS) technique. *International Journal of Applied Earth Observation and Geoinformation*, 52, pp.230-242. DOI: 10.1016/j.jag.2016.06.015

56. Sowter, A., Athab, A., Novellino, A., Grebby, S. and Gee, D., 2018. Supporting energy regulation by monitoring land motion on a regional and national scale: A case study of Scotland. *Proceedings of the Institution of Mechanical Engineers, Part A: Journal of Power and Energy*, *232*(1), pp.85-99. DOI: 10.1177/0957650917737225
57. Sowter, A., Bateson, L., Strange, P., Ambrose, K. and Syafiudin, M.F., 2013. DInSAR estimation of land motion using intermittent coherence with application to the South Derbyshire and Leicestershire coalfields. *Remote Sensing Letters*, *4*(10), pp.979-987. DOI: 10.1080/2150704X.2013.823673
58. Themistocleous, K., Cuca, B., Agapiou, A., Lysandrou, V., Tzouvaras, M., Hadjimitsis, D.G., Kyriakides, P., Kouhartsiouk, D., Margottini, C., Spizzichino, D. and Cigna, F., 2016, October. The Protection of Cultural Heritage Sites from Geo-Hazards: The PROTHEGO Project. In *Euro-Mediterranean Conference* (pp. 91-98). Springer International Publishing. DOI: 10.1007/978-3-319-48974-2_11
59. Torres, R., Snoeij, P., Geudtner, D., Bibby, D., Davidson, M., Attema, E., Potin, P., Rommen, B., Floury, N., Brown, M. and Traver, I.N., 2012. GMES Sentinel-1 mission. *Remote Sensing of Environment*, *120*, pp.9-24. DOI: 10.1016/j.rse.2011.05.028
60. UKRI, 2018. InSAR as a Tool to evaluate Peatland Sensitivity to global change (NE/P014100/1). [online] United Kingdom Research and Innovation. Available at:< http://gtr.ukri.org/projects?ref=NE%2FP014100%2F1> [Accessed 20th April 2018]

61. Van ‘t Hof, W., 2017. *Gas Production from the Groningen Field*. Netherlands Ministry of Economic Affairs. Available at< https://www.unece.org/fileadmin/DAM/energy/se/pdfs/nat_gas/geg/geg4_March2017/Item_4_-_vant_Hof_Groningen_Web.pdf> [Accessed 12th March 2018].

62. Van der Meulen, M.J., Doornenbal, J.C., Gunnink, J.L., Stafleu, J., Schokker, J., Vernes, R.W., Van Geer, F.C., Van Gessel, S.F., Van Heteren, S., Van Leeuwen, R.J.W. and Bakker, M.A.J., 2013. 3D geology in a 2D country: perspectives for geological surveying in the Netherlands. *Netherlands Journal of Geosciences*, *92*(4), pp.217-241. DOI: 10.1017/S0016774600000184

63. Van Thienen-Visser, K. and Breunese, J., 2015. Induced seismicity of the Groningen gas field: history and recent developments, The Leading Edge, special issue Injection Induced Seismicity, pp.665–671. DOI: 10.1190/tle34060664.1

64. Van Thienen-Visser, K., Roholl, J.A., van Kempen, B.M.M. and Muntendam-Bos, A.G., 2018. Categorizing seismic risk for the onshore gas fields in the Netherlands. *Engineering Geology, 237*, pp.198-207. DOI: 10.1016/j.enggeo.2018.02.004

65. Vervoort, A. and Declercq, P.Y., 2017. Upward surface movement above deep coal mines after closure and flooding of underground workings. *International Journal of Mining Science and Technology*, 28, pp.53-59. DOI: 10.1016/j.ijmst.2017.11.008

66. Vonhögen, L.M., Doornenbal, P.J., De Lange, G., Fokker, P.A. & Gunnink, J.L., 2012. Subsidence in the Holocene delta of the Netherlands. *In Proceedings of EISOLS 2010: Land subsidence, Associated Hazards and the role of Natural Resources Development*.

67. Wang, Y, Day, J.L. and Davis, F.W., 1998. Sensitivity of Modeled C- and L-Band Radar Backscatter to Ground Surface Parameters in Loblolly Pine Forest. *Remote Sensing of the Environment*, 66, pp.331-342. DOI: 10.1016/S0034-4257(98)00074-1

68. de Waal, J.A., Muntendam-Bos, A.G. and Roest, J.P.A., 2015. Production induced subsidence in the Groningen gas field – can it be managed? *Proc. IAHS*, *372*, pp.129-139. DOI: 10.5194/piahs-372-129-2015

69. de Waal, J.A., Roest, J.P.A., Fokker, P.A., Kroon, I.C., Breunese, J.N., Muntendam-Bos, A.G., Oost, A.P. and van Wirdum, G., 2012. The effective subsidence capacity concept: How to assure that subsidence in the Wadden Sea remains within defined limits? *Netherlands Journal of Geosciences*, 91-3, pp.385-399. DOI: 10.1017/S0016774600000512

70. Zebker, H.A. and Villasenor, J., 1992. Decorrelation in interferometric radar echoes. *IEEE Transactions on Geoscience and Remote Sensing*, *30*(5), pp.950-959. DOI: 10.1109/36.175330